

1 **Millennial-scale variations of sedimentary oxygenation in the western**
2 **subtropical North Pacific and its links to the North Atlantic climate**

3
4 Jianjun Zou^{1,2}, Xuefa Shi^{1,2}, Aimei Zhu¹, Selvaraj Kandasamy³, Xun Gong⁴, Lester
5 Lembke-Jene⁴, Min-Te Chen⁵, Yonghua Wu^{1,2}, Shulan Ge^{1,2}, Yanguang Liu^{1,2}, Xinru
6 Xue¹, Gerrit Lohmann⁴, Ralf Tiedemann⁴

7 ¹Key Laboratory of Marine Sedimentology and Environmental Geology, First Institute
8 of Oceanography, MNR, Qingdao 266061, China

9 ²Laboratory for Marine Geology, Qingdao National Laboratory for Marine Science
10 and Technology, Qingdao, 266061, China

11 ³Department of Geological Oceanography and State Key Laboratory of Marine
12 Environmental Science, Xiamen University, Xiamen361102, China

13 ⁴Alfred-Wegener-Institut Helmholtz-Zentrum für Polar- und Meeresforschung,
14 Bussestr. 24, 27570 Bremerhaven, Germany

15 ⁵Institute of Applied Geosciences, National Taiwan Ocean University, Keelung 20224,
16 Taiwan

17
18 Corresponding authors:

19 Jianjun Zou (zoujianjun@fio.org.cn); Xuefa Shi (xfshi@fio.org.cn)

20 **Key Points**

21 1. This study reconstructs the history of sedimentary oxygenation processes at
22 mid-depths in the western subtropical North Pacific since the last glacial period.

23 2. Sediment-bound redox-sensitive proxies reveal millennial-scale variations in
24 sedimentary oxygenation that correlated closely to changes in the North Pacific
25 Intermediate Water.

26 3. A millennial-scale out-of-phase relationship between deglacial ventilation in the
27 western subtropical North Pacific and the formation of North Atlantic Deep Water is
28 suggested.

29 4. A larger CO₂ storage at mid-depths of the North Pacific corresponds to the
30 termination of atmospheric CO₂ rise during the Bölling-Alleröd interval.

31 **Abstract**

32 Deep ocean carbon cycle, especially carbon sequestration and outgassing, is one
33 of the competitive mechanisms to explain variations in atmospheric CO₂
34 concentrations on orbital and millennial timescales. However, the potential role of
35 subtropical North Pacific subsurface waters in modulating atmospheric CO₂ levels on
36 millennial timescales is poorly constrained. Further, an increase in respired CO₂
37 concentration in the glacial deep ocean due to biological pump generally corresponds
38 to deoxygenation in the subsurface layer. This link thus offers a chance to visit
39 oceanic ventilation and the coeval export productivity based on redox-controlled,
40 sedimentary geochemical parameters. Here we investigate a suite of geochemical
41 proxies in a sediment core CSH1 to understand the sedimentary oxygenation
42 variations in the subtropical North Pacific over the last 50 thousand years (ka). Our
43 results suggest that enhanced sedimentary oxygenation at mid-depths of the
44 subtropical North Pacific occurred during the cold intervals and after 8.5 ka, while
45 decreased oxygenation during the Bölling-Alleröd (B/A) and Preboreal. The enhanced
46 sedimentary oxygenation in the subtropical North Pacific is aligned with intensified
47 formation of North Pacific Intermediate Water (NPIW) during cold spells, while the
48 ameliorated sedimentary oxygenation seems to be linked to the intensified Kuroshio
49 Current since 8.5 ka. The enhanced formation of NPIW during HS1 can be driven by
50 the perturbation of sea ice formation and sea surface salinity oscillation in
51 high-latitude North Pacific. The diminished sedimentary oxygenation during the B/A
52 due to upwelling of aged, nutrient-rich deep water and enhanced export production,
53 indicates an enhanced CO₂ sequestration at mid-depth waters, along with a slight
54 increase in atmospheric CO₂ concentration. We attribute these millennial-scale
55 changes to intensified NPIW and enhanced abyss flushing during deglacial cold and
56 warm intervals, respectively, on the basis of background climate change due to shift in
57 North Atlantic Deep Water formation.

58 **Keywords:** sedimentary oxygenation; millennial timescale; North Pacific
59 Intermediate Water; North Atlantic Deep Water; subtropical North Pacific

61 **1. Introduction**

62 The sluggish ocean ventilation and efficient biological pump in the ocean
63 facilitate carbon sequestration in the ocean interior, linking to atmospheric CO₂
64 drawdown, which in turn play a crucial role in regulating sedimentary oxygen on
65 millennial and orbital timescales (Hoogakker et al., 2015; Jaccard and Galbraith, 2012;
66 Sigman and Boyle, 2000). Reconstruction of past sedimentary oxygenation is
67 therefore crucial for understanding changes in export productivity and the renewal
68 rate of deep ocean circulation (Nameroff et al., 2004). Previous studies from eastern
69 and western North Pacific margins and subarctic Pacific have identified drastic
70 variations in export productivity and ocean oxygen levels at glacial-interglacial
71 timescales using diverse proxies such as trace elements (Cartapanis et al., 2011;
72 Chang et al., 2014; Jaccard et al., 2009; Zou et al., 2012), benthic foraminiferal
73 assemblages (Ohkushi et al., 2016; Ohkushi et al., 2013; Shibahara et al., 2007) and
74 nitrogen isotopic composition ($\delta^{15}\text{N}$) of organic matter (Addison et al., 2012; Chang
75 et al., 2014; Galbraith et al., 2004; Riethdorf et al., 2016) in marine sediment cores.
76 These studies further suggested that both North Pacific Intermediate Water (NPIW)
77 and export of organic matter regulate the sedimentary oxygenation variation during
78 the last glaciation and Holocene in the subarctic North Pacific. By contrast, little
79 information exists on millennial-scale oxygenation changes to date in the western
80 subtropical North Pacific.

81 The modern NPIW is mainly sourced from the NW Pacific marginal seas
82 (Shcherbina et al., 2003; Talley, 1993; You et al., 2000), and then it spreads into
83 subtropical North Pacific at intermediate depths of 300 to 800 m (Talley, 1993). The
84 pathway and circulation of NPIW have been identified by You (2003), who suggested
85 that cabbeling, a mixing process to form a new water mass with increased density
86 than that of parent water masses, is the principle mechanism responsible for
87 transforming subpolar source waters into subtropical NPIW along the
88 subarctic-tropical frontal zone. More specifically, You et al. (2003) argued that a
89 lower subpolar input of about 2 Sv (1 Sv = 10⁶ m³/s) is sufficient for subtropical
90 ventilation. Benthic foraminiferal $\delta^{13}\text{C}$, a quasi-conservative tracer for water mass,

91 from the North Pacific suggested an enhanced ventilation (enriched $\delta^{13}\text{C}$) at water
92 depths of < 2000 m during the last glacial period (Keigwin, 1998; Matsumoto et al.,
93 2002). Furthermore, on the basis of both radiocarbon data and modeling results,
94 Okazaki et al. (2010) provided further insight into the formation of deep water in the
95 North Pacific during early deglaciation. Enhanced NPIW penetration is further
96 explored using numerical model simulations (Chikamoto et al., 2012; Gong et al.,
97 2019; Okazaki et al., 2010). More recently, Max et al (2017) identified the substantial
98 effects of intensified NPIW on $\delta^{13}\text{C}$ of deep-dwelling planktic foraminifera
99 *Globorotaloides hexagonus* in the Eastern Equatorial Pacific during Marine Isotope
100 Stage (MIS) 2. Subsequently, Rippert et al. (2017) confirmed that such enhanced
101 effect of NPIW also occurred during MIS 6. The downstream effects of intensified
102 NPIW also can be seen in the record of $\delta^{13}\text{C}$ of *Cibicides wuellerstorfi* in core PN-3
103 from the middle Okinawa Trough (OT), whereas lower deglacial $\delta^{13}\text{C}$ values were
104 attributed to enhanced OC accumulation rates due to higher surface productivity by
105 Wahyudi and Minagawa (1997).

106 The Okinawa Trough is separated from the Philippine Sea by the Ryukyu Islands
107 and is an important channel of the northern extension of the Kuroshio in the western
108 subtropical North Pacific (Figure 1). Initially the OT opened at the middle Miocene
109 (Sibuet et al., 1987) and since then, it has been a depositional center in the East China
110 Sea (ECS), receiving large sediment supplies from nearby rivers (Chang et al., 2009).
111 Surface hydrographic characteristics of the OT over glacial-interglacial cycles are
112 largely influenced by the Kuroshio and ECS Coastal Water (Shi et al., 2014); the latter
113 is related to the strength of summer East Asian monsoon (EAM) sourced from the
114 western tropical Pacific. Modern physical oceanographic investigations showed that
115 intermediate waters in the OT are mainly derived from horizontal advection and
116 mixture of NPIW and South China Sea Intermediate Water (Nakamura et al., 2013).
117 These waters intrude into the OT through two ways: (i) deeper part of the Kuroshio
118 enters the OT through the channel east of Taiwan (sill depth 775 m) and (ii) through
119 the Kerama Gap (sill depth 1100 m). In the northern OT, the occupied subsurface
120 water mainly flows through the Kerama Gap through horizontal advection from the

121 Philippine Sea (Nakamura et al., 2013). Recently, Nishina et al. (2016) found that an
122 overflow through the Kerama Gap controls the modern deep-water ventilation in the
123 southern OT.

124 Both surface hydrography and deep ventilation in the OT varied greatly since the
125 last glaciation. During the last glacial periods, the mainstream of the Kuroshio likely
126 migrated to the east of the Ryukyu Islands or and also became weaker due to lower
127 sea levels (Shi et al., 2014; Ujiie and Ujiie, 1999; Ujiie et al., 2003) and the
128 hypothetical emergence of a Ryukyu-Taiwan land bridge (Ujiie and Ujiie, 1999). In a
129 recent study, based on the Mg/Ca-derived temperatures in surface and thermocline
130 waters and planktic foraminiferal indicators of water masses from two sediment cores
131 located in the northern and southern OT, Ujiie et al. (2016) argued that the
132 hydrological conditions of North Pacific Subtropical Gyre since MIS 7 is modulated
133 by the interaction between the Kuroshio and the NPIW. Besides the Kuroshio, the
134 flux of East Asian rivers to the ECS, which is related to the summer EAM and the sea
135 level oscillations coupled with topography have also been regulating the surface
136 hydrography in the OT (Chang et al., 2009; Kubota et al., 2010; Sun et al., 2005; Yu
137 et al., 2009).

138 Based on benthic foraminiferal assemblages, previous studies have implied a
139 reduced oxygenation in deep waters of the middle and southern OT during the last
140 deglacial period (Jian et al., 1996; Li et al., 2005), but a strong ventilation during the
141 Last Glacial Maximum (LGM) and the Holocene (Jian et al., 1996; Kao et al., 2005).
142 High sedimentary $\delta^{15}\text{N}$ values, an indicator of increased denitrification in the
143 subsurface water column, also occurred during the late deglaciation in the middle OT
144 (Kao et al., 2008). Inconsistent with these results, Dou et al. (2015) suggested an oxic
145 depositional environment during the last deglaciation in the southern OT based on
146 weak positive cerium anomalies. Furthermore, Kao et al. (2006) concluded a reduced
147 ventilation of deepwater in the OT during the LGM due to the reduction of KC inflow
148 using a 3-D ocean model. Yet, the patterns and reasons that caused sedimentary
149 oxygenation in the OT thus remain unclear.

150 **2. Paleo-redox proxies**

151 Sedimentary redox condition is governed by the rate of oxygen supply from the
152 overlying bottom water and the rate of oxygen removal from pore water (Jaccard et al.,
153 2016), processes that are related to the supply of oxygen by ocean circulation and
154 organic matter respiration, respectively. Contrasting geochemical behaviors of
155 redox-sensitive trace metals (Mn, Mo, U, etc.) have been used to reconstruct bottom
156 water and sedimentary oxygen changes (Algeo, 2004; Algeo and Lyons, 2006;
157 Crusius et al., 1996; Dean et al., 1997; Tribovillard et al., 2006; Zou et al., 2012), as
158 their concentrations readily respond to redox condition of the depositional
159 environment (Morford and Emerson, 1999).

160 In general, enrichment of Mn with higher speciation states (Mn (III) and Mn (IV))
161 in the form of Mn-oxide coatings is observed in marine sediments, when oxic
162 condition prevails into greater sediment depths as a result of low organic matter
163 degradation rates and well-ventilated bottom water (Burdige, 1993). Under reducing
164 conditions, the authigenic fraction of Mn (as opposed to its detrital background) is
165 released as dissolved Mn (II) species into the pore water and thus its concentration is
166 usually low in suboxic (O_2 and HS^- absent) and anoxic (HS^- present) sediments. In
167 addition, when Mn enrichment occurs in oxic sediments as solid phase Mn
168 oxyhydroxides, it may lead to co-precipitation of other elements, such as Mo
169 (Nameroff et al., 2002).

170 The elements Mo and U behave conservatively in oxygenated seawater, but are
171 preferentially enriched in oxygen-depleted water (Morford and Emerson, 1999).
172 However, these two trace metals behave differently in several ways. Molybdenum can
173 be enriched in both oxic sediments, such as the near surface manganese-rich horizons
174 in continental margin environments (Shimmiel and Price, 1986) and in anoxic
175 sediments (Nameroff et al., 2002). Under anoxic conditions, Mo can be reduced either
176 from the +6 oxidation state to insoluble MoS_2 , though this process is known to occur
177 only under extremely reducing conditions, such as hydrothermal and/or diagenesis
178 (Dahl et al., 2010; Helz et al., 1996) or be converted to particle-reactive
179 thiomolybdates (Vorlicek and Helz, 2002). Zheng et al. (2000) suggested two critical
180 thresholds for Mo scavenging from seawater: 0.1 μM hydrogen sulfide (H_2S) for

181 Fe-S-Mo co-precipitation and 100 μM H_2S for Mo scavenging as Mo-S or as
182 particle-bound Mo without Fe. Although Crusius et al. (1996) noted insignificant
183 enrichment of sedimentary Mo under suboxic conditions, Scott et al. (2008) argued
184 that burial flux of Mo is not so low in suboxic environments. Excess concentration of
185 Mo ($\text{Mo}_{\text{excess}}$) in sediments thus suggests the accumulation of sediments either in
186 anoxic (H_2S occurrence) or well oxygenated conditions (if $\text{Mo}_{\text{excess}}$ is in association
187 with Mn-oxides).

188 In general, U is enriched in anoxic sediments ($>1 \mu\text{M}$ H_2S), but not in oxic
189 sediments ($>10 \mu\text{M}$ O_2) (Nameroff et al., 2002). Accumulation of U depends on the
190 content of reactive organic matter (Sundby et al., 2004) and U precipitates as uraninite
191 (UO_2) during the conversion of Fe (III) to Fe (II) in suboxic conditions (Morford and
192 Emerson, 1999; Zheng et al., 2002). One of the primary removal mechanisms for U
193 from the ocean is via diffusion across the sediment-water interface of reducing
194 sediments (Klinkhammer and Palmer, 1991). Under suboxic conditions, soluble U (VI)
195 is reduced to insoluble U (IV), but free sulfide is not required for U precipitation
196 (McManus et al., 2005). Jaccard et al. (2009) suggested that the presence of excess
197 concentration of U (U_{excess}) in the absence of Mo enrichment is indicative of a suboxic,
198 but not sulfidic condition, within the diffusional range of the sediment-water interface.
199 The felsic volcanism is also a primary source of uranium (Maithani and Srinivasan,
200 2011). Therefore, the potential input of uranium from active volcanic sources around
201 the northwestern Pacific to the adjacent sediments should not be neglected.

202 In this study, we investigate a suite of redox-sensitive elements and the ratio of
203 Mo/Mn along with productivity proxies from a sediment core retrieved from the
204 northern OT to reconstruct the sedimentary oxygenation in the western subtropical
205 North Pacific over the last 50ka. Based on that, we propose that multiple factors, such
206 as NPIW ventilation, the strength of the Kuroshio Current and export productivity,
207 control the bottom sedimentary oxygenation in the OT on millennial timescales since
208 the last glacial.

209 **3. Oceanographic setting**

210 Surface hydrographic characteristics of the OT are mainly controlled by the

211 warmer, more saline, oligotrophic Kuroshio water and cooler, less saline, nutrient-rich
212 Changjiang Diluted Water, and the modern flow-path of the former is influenced by
213 the bathymetry of the OT (Figure 1a). The Kuroshio Current originates from the
214 North Equatorial Current and flows into the ECS from the Philippine Sea through the
215 Suao-Yonaguni Depression. In the northern OT, Tsushima Warm Current (TWC), a
216 branch of the Kuroshio, flows into the Japan Sea through the shallow Tsushima Strait.
217 Volume transport of the Kuroshio varies seasonally due to the influence of the EAM
218 with a maximum of 24 Sv in summer and a minimum of 20 Sv in autumn across the
219 east of Taiwan (Qu and Lukas, 2003).

220 Figures 2a and 2b show that the lower sea surface salinity (SSS) zone in summer
221 relative to the one in winter in the ECS migrates toward the east of OT, indicating
222 enhanced impact of the Changjiang discharge associated with summer EAM. An
223 estimated ~80% of the mean annual discharge of Changjiang is supplied to the ECS
224 (Ichikawa and Beardsley, 2002) and in situ observational data show a pronounced
225 negative correlation between the Changjiang discharge and SSS in July (Delcroix and
226 Murtugudde, 2002). Consistently, previous studies from the OT reported such close
227 relationship between summer EAM and SSS back to the late Pleistocene (Chang et al.,
228 2009; Clemens et al., 2018; Kubota et al., 2010; Sun et al., 2005).

229 Despite the effects of EAM and the Kuroshio, evidence of geochemical tracers
230 (temperature, salinity, oxygen, nutrients and radiocarbon- $\Delta^{14}\text{C}$) collected during the
231 World Ocean Circulation Experiment (WOCE) Expeditions in the Pacific (transects
232 P24 and P03) favors the presence of low saline, nutrient-enriched intermediate and
233 deep waters (Talley, 2007). Dissolved oxygen content is $<100 \mu\text{mol/kg}$ at water
234 depths of below 600 m in the OT along WOCE transects PC03 and PC24 (Talley,
235 2007). Modern oceanographic observations at the Kerama Gap reveal that upwelling
236 in the OT is associated with the inflow of NPIW and studies using box model
237 predicted that overflow through the Kerama Gap is responsible for upwelling ($3.8\text{--}7.6$
238 $\times 10^{-6} \text{m s}^{-1}$) (Nakamura et al., 2013; Nishina et al., 2016).

239 **4. Materials and methods**

240 **4.1. Chronostratigraphy of core CSH1**

241 A 17.3 m long sediment core CSH1 (31° 13.7' N, 128° 43.4' E; water depth: 703
242 m) was collected from the northern OT, close to the main stream of Tsushima Warm
243 Current (TWC) (Figure 1b) and within the depth of NPIW (Figure 1c) using a piston
244 corer during *Xiangyanghong09* Cruise in 1998. This location is thus enabling us to
245 reconstruct millennial-scale changes in the properties of TWC and NPIW. The
246 expedition was carried out by the First Institute of Oceanography, Ministry of Natural
247 Resources of China. Core CSH1 mainly consists of clayey silt and silt with
248 occurrence of plant debris at some depth intervals (Ge et al., 2007) (Figure 3a). In
249 addition, three layers of volcanic ash were observed at depths of 74–106 cm, 782–794
250 cm, 1570–1602 cm and these three intervals can be correlated with well-known ash
251 layers, Kikai-Akahoya (K-Ah; 7.3 ka), Aira-Tanzawa (AT; 29.24 ka) and Aso-4
252 (roughly around MIS 5a) (Machida, 1999), respectively. The core was split and
253 sub-sampled at every 4 cm interval and then stored in China Ocean Sample
254 Repository at 4 °C until analysis.

255 Previously, some paleoceanographic studies have been conducted and a set of
256 data have been investigated for core CSH1, including the contents of planktic
257 foraminifers as well as their carbon ($\delta^{13}\text{C}$) and oxygen isotope ($\delta^{18}\text{O}$) compositions
258 (Shi et al., 2014), pollen (Chen et al., 2006), paleomagnetism (Ge et al., 2007) and
259 CaCO_3 (Wu et al., 2004). An age model for this core has been constructed by using
260 ten Accelerator Mass Spectrometry (AMS) ^{14}C dates and six oxygen isotope ($\delta^{18}\text{O}$)
261 age control points. The whole 17.3 m core contains *ca.* 88 ka-long record of
262 continuous sedimentation (Shi et al., 2014).

263 It is noteworthy that previous age control points with constant radiocarbon
264 reservoir throughout core CSH1 are used to reveal orbital-scale Kuroshio variations
265 (Shi et al., 2014), but insufficient to investigate millennial-scale climatic events. On
266 the basis of original age model, a higher abundance of *Neogloboquadrina*
267 *pachyderma* (dextral) that occurred during warmer intervals, such as the B/A, has
268 been challenging to explain reasonably. On the other hand, paired measurements of
269 $^{14}\text{C}/^{12}\text{C}$ and ^{230}Th ages from Hulu Cave stalagmites suggest magnetic field change has
270 greatly contributed to high atmospheric $^{14}\text{C}/^{12}\text{C}$ values at HS4 and the YD (Cheng et

271 al., 2018). Thus a constant reservoir age assumed when calibrating foraminiferal
272 radiocarbon dates using CALIB 6 software and the Marine 13 calibration dataset
273 (Reimer et al., 2013) for core CSH1 may cause large chronological uncertainties.

274 Here, we therefore recalibrated the radiocarbon dates using CALIB 7.04 software
275 with Marine 13 calibration dataset (Reimer et al., 2013). Moreover, on the basis of
276 significant correlation between planktic foraminifera species *Globigerinoides ruber*
277 $\delta^{18}\text{O}$ and Chinese stalagmite $\delta^{18}\text{O}$ (Cheng et al., 2016), a proxy of summer EAM
278 related to SSS of the ECS, we re-established the age model for core CSH1 (Figures
279 3b-d). Overall, the new chronological framework is similar to the one previously
280 reported by Shi et al. (2014), but with more dates. In order to compare with published
281 results associated with ventilation changes in the North Pacific, here we mainly report
282 the history of sedimentary oxygenation in the northern OT since the last glacial period.
283 Linear sedimentation rate varied between ~ 10 and 40 cm/ka with higher
284 sedimentation rate (around $30\text{-}40$ cm/ka) between ~ 24 ka and 32.5 ka. The age control
285 points were shown in Table 2.

286 **4.2. Chemical analyses**

287 Sediment subsamples for geochemical analyses were freeze-dried and ground to
288 a fine powder with an agate mortar and pestle. Based on the age model, 85
289 subsamples from core CSH1 with time resolution of about 600 years (every 4 cm
290 interval) were selected for detailed geochemical analyses of major and minor
291 elements and total contents of carbon (TC), organic carbon (TOC) and nitrogen (TN).
292 The pretreatment of sediment and other analytical methods have been reported
293 elsewhere (Zou et al., 2012).

294 TC and TN were determined with an elemental analyzer (EA; Vario EL III,
295 Elementar Analysen systeme GmbH) in the Key Laboratory of Marine Sediment and
296 Environment Geology, First Institute of Oceanography, Ministry of Natural Resources
297 of China, Qingdao. Carbonate was removed from sediments by adding 1M HCl to the
298 homogenized sediments for total organic carbon (TOC) analysis using the same
299 equipment. The content of calcium carbonate (CaCO_3) was calculated using the
300 equation:

301 $\text{CaCO}_3 = (\text{TC} - \text{TOC}) \times 8.33$

302 where 8.33 is the ratio between the molecular weight of carbonate and the atomic
303 weight of carbon. National reference material (GSD-9), blank sample and replicated
304 samples were used to control the analytical process. The relative standard deviation of
305 the GSD-9 for TC, TN and TOC is $\leq 3.4\%$.

306 About 0.5 g of sediment powder was digested in double distilled HF:HNO₃ (3:1),
307 followed by concentrated HClO₄, and then re-dissolved in 5% HNO₃. Selected major
308 and minor elements such as aluminum (Al) and manganese (Mn) were determined by
309 inductively coupled plasma optical emission spectroscopy (ICP-OES; Thermo
310 Scientific iCAP 6000, Thermo Fisher Scientific), as detailed elsewhere (Zou et al.,
311 2012). In addition, Mo and U were analyzed with inductively coupled plasma mass
312 spectrometry (ICP-MS; Thermo Scientific XSERIES 2, Thermo Fisher Scientific), as
313 described in Zou et al. (2012). Precision for most elements in the reference material
314 GSD-9 is $\leq 5\%$ relative standard deviation. The excess fractions of U and Mo were
315 estimated by normalization to Al:

316 $\text{Excess fraction} = \frac{\text{total}_{\text{element}}}{\text{Al}_{\text{average shale}}} - (\text{element}/\text{Al}_{\text{average shale}} \times \text{Al})$, with $\text{U}/\text{Al}_{\text{average shale}} =$
317 0.307×10^{-6} and $\text{Mo}/\text{Al}_{\text{average shale}} = 0.295 \times 10^{-6}$ (Li and Schoonmaker, 2014).

318 In addition, given the different geochemical behaviors of Mn and Mo and
319 co-precipitation and adsorption processes associated with the redox cycling of Mn, we
320 calculated the ratio of Mo to Mn, assuming that higher Mo/Mn ratio indicates lower
321 oxygen content in the depositional environment and vice versa. In combination with
322 the concentration of excess uranium, we infer the history of sedimentary oxygenation
323 in the subtropical North Pacific since the last glaciation.

324 **5. Results**

325 **5.1. TOC, TN, and CaCO₃**

326 The content of CaCO₃ varies from 8.8 to 35% (Figure 4a) and it mostly shows
327 higher values with increasing trends during the last deglaciation. In contrast, the
328 content of CaCO₃ is low and exhibits decreasing trends during the late MIS 3 and the
329 LGM (Figure 4a). TN content shows a larger variation compared to TOC (Figure 4b),
330 but it still strongly correlates with TOC ($r = 0.74$, $p < 0.01$) throughout the entire core.

331 Concentration of TOC ranges from 0.5 to 2.1% and it shows higher values with stable
332 trends during the last glacial phase (MIS 3) (Figure 4c). Molar ratios of TOC/TN vary
333 around 10, with higher ratios at the transition into the LGM (Figure 4d),
334 corresponding to higher linear sedimentation rate (Figure 4e).

335 Both TOC and CaCO₃ have been used as proxies for the reconstruction of past
336 export productivity (Cartapanis et al., 2011; Lembke-Jene et al., 2017; Rühlemann et
337 al., 1999). Molar C/N ratios of >10 (Figure 4c) suggest that terrigenous organic
338 sources significantly contribute to the TOC concentration in core CSH1. The TOC
339 content therefore may be not a reliable proxy for the reconstruction of surface water
340 export productivity during times of the LGM and late deglaciation, when maxima in
341 C/N ratios co-occur with decoupled trends between CaCO₃ and TOC concentrations.

342 Several lines of evidence support CaCO₃ as a reliable productivity proxy,
343 particularly during the last deglaciation. The strong negative correlation coefficient (r
344 = - 0.85, $p < 0.01$) between Al and CaCO₃ in sediments throughout core CSH1
345 confirms the biogenic origin of CaCO₃ against terrigenous Al (Figure 4f). Generally,
346 terrigenous dilution decreases the concentrations of CaCO₃. Inconsistent relationship
347 between percentage CaCO₃ and sedimentation rate indicates a minor effect of dilution
348 on CaCO₃. Furthermore, the increasing trend in CaCO₃ associated with high
349 sedimentation rate during the last deglacial interval indicates a substantial increase in
350 export productivity (Figures 4a and 4d). The high coherence between percentage
351 CaCO₃ and alkenone-derived sea surface water (SST) (Shi et al., 2014) indicates a
352 direct control on CaCO₃ by SST. Finally, a detailed comparison between CaCO₃
353 concentrations and the previously published foraminiferal fragmentation ratio (Wu et
354 al., 2004) shows, apart from a small portion within the LGM, no clear co-variation
355 between them. These evidence suggest that CaCO₃ changes are driven primarily by
356 variations in carbonate primary production, and not overprinted by secondary
357 processes, such as carbonate dissolution through changes in the lysocline depth and
358 dilution by terrigenous materials. Likewise, similar deglacial trend in CaCO₃ is also
359 observed in core MD01-2404 (Chang et al., 2009), indicating a ubiquitous, not local
360 picture in the OT. All these lines of evidence thus support CaCO₃ of core CSH1 as a

361 reliable productivity proxy to a first order approximation.

362 **5.2. Redox-sensitive Elements**

363 Figure 4 shows time series of selected redox-sensitive elements (RSEs) and
364 proxies derived from them. Mn shows higher concentrations during the LGM and
365 HS1 (16 ka–22.5 ka) and middle-late Holocene, but lower concentrations during the
366 last deglacial and Preboreal periods (15.8 ka–9.5 ka) (Figure 4g). Generally,
367 concentrations of excess Mo and excess U (Figures 4j and 4l) show coherent patterns
368 with those of Mo and U (Figures 4i and 4k), but both are out-of-phase with Mn over
369 the last glacial period (Figure 4h). It should be noted that pronounced variations in U
370 concentration since 8.5 ka is related to the occurrence of discrete volcanic materials. A
371 significant positive Eu anomaly (Zhu et al., 2015) together with more radiogenic Nd
372 values (unpublished data) from the same core confirms the occurrence of discrete
373 volcanic materials and its dilution effects on terrigenous components since 7 ka.
374 Occurrence of discrete volcanic material is likely related to intensified Kuroshio
375 Current during the mid-late Holocene, as supported by higher hydrothermal Hg
376 concentrations in sediments from the middle OT (Lim et al., 2017). A negative
377 correlation between Mn and $\text{Mo}_{\text{excess}}$ during the last glaciation and the Holocene, and
378 the strong positive correlation between them during the LGM and HS1 (Figures 5a
379 and 5b) further corroborate the complicated geochemical behaviors of Mn and Mo. A
380 strong positive correlation between $\text{Mo}_{\text{excess}}$ and Mn (Figure 5b) may be attributed to
381 co-precipitation of Mo by Mn-oxyhydroxide under oxygenated conditions. Here, we
382 use Mo/Mn ratio, instead of excess Mo concentration to reconstruct variations in
383 sedimentary redox conditions in the study area. Overall, the Mo/Mn ratio shows
384 similar downcore pattern to that of $\text{Mo}_{\text{excess}}$ with higher ratios during the last
385 deglaciation, but lower ratios during the LGM and HS1. A strong correlation ($r = 0.69$)
386 between Mo/Mn ratio and excess U concentration (excluding the data of Holocene,
387 due to contamination of volcanic material, Figure 5c) further corroborates the
388 integrity of Mo/Mn as an indicator of sedimentary oxygenation changes.

389 Rapidly decreasing Mo/Mn ratio indicates an oxygenated sedimentary
390 environment since ~ 8 ka (Figure 4h). Both higher Mo/Mn ratios and excess U

391 concentration, together with lower Mn concentrations suggest a deoxygenated
392 depositional condition during the late deglacial period (15.8 ka–9.5 ka), whereas
393 lower ratios during the LGM, HS1 and HS2 indicate relatively better oxygenated
394 sedimentary condition. A decreasing trend in Mo/Mn ratio and excess U concentration
395 from 50 ka to 25 ka also suggest higher sedimentary oxygen levels.

396 **6. Discussion**

397 **6.1. Constraining paleoredox conditions in the Okinawa Trough**

398 In general, three different terms, hypoxia, suboxia and anoxia, are widely used to
399 describe the degree of oxygen depletion in the marine environment (Hofmann et al.,
400 2011). Here, we adopt the definition of oxygen thresholds by Bianchi et al. (2012) for
401 oxic ($>120 \mu\text{mol/kg O}_2$), hypoxic ($<60\text{--}120 \mu\text{mol/kg O}_2$) and suboxic ($<2\text{--}10$
402 $\mu\text{mol/kg O}_2$) conditions, whereas anoxia is the absence of measurable oxygen.

403 Proxies associated with RSEs, such as sedimentary Mo concentration (Lyons et
404 al., 2009; Scott et al., 2008) have been used to constrain the degree of oxygenation in
405 seawater. Algeo and Tribovillard (2009) proposed that open-ocean systems with
406 suboxic waters tend to yield U_{excess} enrichment relative to Mo_{excess} , resulting in
407 sediment $(Mo/U)_{\text{excess}}$ ratio less than that of seawater (7.5–7.9). Under increasingly
408 reducing and occasionally sulfidic conditions, the accumulation of Mo_{excess} increase
409 relative to that of U_{excess} leading the $(Mo/U)_{\text{excess}}$ ratio either is equal to or exceeds
410 with that of seawater. Furthermore, Scott and Lyons (2012) suggested a non-euxinic
411 condition with the presence of sulfide in pore waters, when Mo concentrations range
412 from $> 2 \mu\text{g/g}$, the crustal average to $< 25 \mu\text{g/g}$, a threshold concentration for euxinic
413 condition. Given that the northern OT is located in the open oceanic settings, we use
414 these two above mentioned proxies to evaluate the degree of oxygenation in
415 sediments.

416 Both bulk Mo concentration (1.2–9.5 $\mu\text{g/g}$) and excess (Mo/U) ratio (0.2–5.7) in
417 core CSH1 suggest that oxygen-depleted conditions may have prevailed in the deep
418 water of the northern OT over the last 50 ka (Figure 4m). However, increased excess
419 Mo concentration with enhanced Mo/U ratio during the last termination (18ka–9 ka)
420 indicate a stronger reducing condition compared to the Holocene and the last glacial

421 period, though Mo concentration is less than 25 $\mu\text{g/g}$, a threshold for euxinic
422 deposition proposed by Scott and Lyons (2012).

423 The relative abundance of benthic foraminifera species that thrive in different
424 oxygen concentrations also have been widely used to reconstruct the variations in
425 bottom water ventilation, such as enhanced abundance of *Bulimina aculeata*,
426 *Uvigerina peregrina* and *Chilostomella oolina* found under oxygen-depleted
427 conditions in the central and southern OT during the last deglaciation (18 ka -9.2 ka)
428 (Jian et al., 1996; Li et al., 2005). An oxygenated bottom water condition is also
429 indicated by abundant benthic foraminifera species *Cibicidoides hyalina* and
430 *Globocassidulina subglobosa* after 9.2 ka (Jian et al., 1996; Li et al., 2005) in cores
431 E017 (1826 m water depth), 255 (1575 m water depth) and high benthic $\delta^{13}\text{C}$ values
432 (Wahyudi and Minagawa, 1997) in core PN-3 (1058 m water depth) from the middle
433 and southern OT during the postglacial period. The poorly-ventilated deep water in
434 the middle and southern OT inferred by benthic foraminiferal assemblages during the
435 last deglaciation is coeval with the one in the northern OT referring to our RSEs
436 (Figure 4). A clear linkage thus can be established between deep-water ventilation and
437 sedimentary oxygenation in the OT. Overall, a combination of our proxy records of
438 RSEs in core CSH1 with other records shows oxygen-rich conditions during the last
439 glaciation and middle and late Holocene (since 8.5 ka) intervals, but oxygen-poor
440 conditions during the last deglaciation.

441 **6.2. Causes for sedimentary oxygenation variations**

442 As discussed above, the pattern of RSEs in core CSH1 suggests that drastic
443 changes in sedimentary oxygenation occurred on orbital and millennial timescales
444 over the last glaciation in the OT. In general, four factors can regulate the redox
445 condition in the deep water column: (i) O_2 solubility, (ii) export productivity and
446 subsequent degradation of organic matter, (iii) vertical mixing, and (iv) lateral supply
447 of oxygen through intermediate and deeper water masses (Ivanochko and Pedersen,
448 2004; Jaccard and Galbraith, 2012). These processes have been invoked in previous
449 studies to explain the deglacial Pacific-wide variations in oxygenation by either one or
450 a combination of these factors (Galbraith and Jaccard, 2015; Moffitt et al., 2015;

451 Praetorius et al., 2015). Our data also suggest drastic variations in sedimentary
452 oxygenation over the last 50 ka. However, the mechanisms responsible for
453 sedimentary oxygenation variations in the basin-wide OT and its connection with
454 ventilation of the open North Pacific remain unclear. In order to place our core results
455 in a wider regional context, here, we compare our proxy records of sedimentary
456 oxygenation (U_{excess} concentration and Mo/Mn ratio) and export productivity (CaCO_3)
457 (Figures 6a, b, c) with abundance of *Pulleniatina obliquiloculata* (an indicator of
458 Kuroshio strength) and sea surface temperature (Shi et al., 2014), bulk sedimentary
459 nitrogen isotope (an indicator of denitrification) (Kao et al., 2008), benthic
460 foraminifera $\delta^{13}\text{C}$ (a proxy for water mass) in cores PN-3 and PC23A (Rella et al.,
461 2012; Wahyudi and Minagawa, 1997), abundance of benthic foraminifera (an
462 indicator of hypoxia) in core E017 (Li et al., 2005) and ODP167 site 1017 (Cannariato
463 and Kennett, 1999) (Figures 6d - k).

464 **6.2.1. Effects of regional ocean temperature on deglacial deoxygenation**

465 Warming ocean temperatures lead to lower oxygen solubility. In the geological
466 past, solubility effects connected to temperature changes of the water column thought
467 to enhance or even trigger hypoxia (Praetorius et al., 2015). Shi et al. (2014) reported
468 an increase in SST of around 4°C ($\sim 21^\circ\text{C}$ to $\sim 24.6^\circ\text{C}$) during the last deglaciation in
469 core CSH1 (Figure 6d). Based on thermal solubility effects, a hypothetical warming
470 of 1°C would reduce oxygen concentrations by about $3.5 \mu\text{mol/kg}$ at water
471 temperatures around 22°C (Brewer and Peltzer, 2016), therefore a $\sim 4^\circ\text{C}$ warming at
472 core CSH1 (Shi et al., 2014) could drive a conservative estimate of a drop of <15
473 $\mu\text{mol/kg}$ in oxygen concentration, assuming no large salinity changes. However,
474 given the semi-quantitative nature of our data about oxygenation changes, which
475 seemingly exceed an amplitude of $>15 \mu\text{mol/kg}$, we suggest that other factors, e.g.
476 local changes in export productivity, regional influences such as vertical mixing due
477 to changes of the Kuroshio Current, and far-field effects may have played decisive
478 roles in shaping the oxygenation history of the OT.

479 **6.2.2. Links between deglacial primary productivity and sedimentary** 480 **deoxygenation**

481 Previous studies have suggested the occurrence of high primary productivity in
482 the entire OT during the last deglacial period (Chang et al., 2009; Jian et al., 1996;
483 Kao et al., 2008; Li et al., 2017; Shao et al., 2016; Wahyudi and Minagawa, 1997).
484 Such an increase in export production was due to favorable conditions for bloom
485 development, which were likely induced by warm temperatures and maxima in
486 nutrient availability, the latter being mainly sourced from increased discharge of the
487 Changjiang River, erosion of material from the ongoing flooding of the shallow
488 continental shelf in the ECS, and upwelling of Kuroshio Intermediate Water (Chang
489 et al., 2009; Li et al., 2017; Shao et al., 2016; Wahyudi and Minagawa, 1997). On the
490 basis of sedimentary reactive phosphorus concentration, Li et al. (2017) concluded
491 that export productivity increased during warm episodes but decreased during cold
492 spells on millennial timescales over the last 91 ka in the OT. Gradually increasing
493 concentrations of CaCO₃ in core CSH1 during the deglaciation (Figure 6a) and little
494 changes in foraminiferal fragmentation ratios (Wu et al., 2004), are indicative of high
495 export productivity in the northern OT. Accordingly, our data indicate that an increase
496 in export productivity during the last deglaciation, which was previously evidenced by
497 concentrations of reactive phosphorus (Li et al., 2017) and CaCO₃ (Chang et al., 2009)
498 from the middle OT, and thus was a pervasive, synchronous phenomenon of entire
499 study region at the outermost extension of the ECS.

500 Similar events of high export productivity have been reported in the entire North
501 Pacific due to increased nutrient supply, high SST, reduced sea ice cover, etc.
502 (Crusius et al., 2004; Dean et al., 1997; Galbraith et al., 2007; Jaccard and Galbraith,
503 2012; Kohfeld and Chase, 2011). In most of these cases, increased productivity were
504 thought to be responsible for oxygen depletion in mid-depth waters, due to
505 exceptionally high oxygen consumption. However, the productivity changes during
506 the deglacial interval, very specifically CaCO₃, are not fully consistent with the trends
507 of excess U and Mo/Mn ratio (Figures 6b and 6c). The sedimentary oxygenation thus
508 cannot be determined by export productivity alone.

509 **6.2.3 Effects of the Kuroshio dynamics on sedimentary oxygenation**

510 The Kuroshio Current, one of the main drivers of vertical mixing, has been

511 identified as the key factor in controlling modern deep ventilation in the OT (Kao et
512 al., 2006). However, the flow path of the Kuroshio in the OT during the glacial
513 interval remains a matter of debate. Planktic foraminiferal assemblages in sediment
514 cores from inside and outside the OT indicated that the Kuroshio have migrated to the
515 east of the Ryukyu Islands during the LGM (Ujiié and Ujiié, 1999). Subsequently,
516 Kao et al. (2006) based on modeling results suggested that the Kuroshio still enters
517 into the OT, but the volume transport was reduced by 43% compared to the
518 present-day transport and the outlet of Kuroshio switches from the Tokara Strait to the
519 Kerama Gap at -80 and -135m lowered sea level. Combined with sea surface
520 temperature (SST) records and ocean model results, Lee et al. (2013) argued that there
521 was little effect of deglacial sea-level change on the path of the Kuroshio, which still
522 exited the OT from the Tokara Strait during the glacial period. Because the main
523 stream of the Kuroshio Current is at a water depth of ~150 m, the SST records are
524 insufficient to decipher past changes of the Kuroshio (Ujiié et al., 2016). On the other
525 hand, low abundances of *P. obliquiloculata* in core CSH1 in the northern OT (Figure
526 6e) indicate that the main flow path of the Kuroshio may have migrated to the east of
527 the Ryukyu Island (Shi et al., 2014). Such a flow change would have been caused by
528 the proposed block of the Ryukyu-Taiwan land bridge by low sea level (Ujiié and
529 Ujiié, 1999) and an overall reduced Kuroshio intensity (Kao et al., 2006), effectively
530 suppressing the effect of the Kuroshio on deep ventilation in the OT. Our RSEs data
531 show that oxygenated sedimentary conditions were dominant in the northern OT
532 throughout the last glacial period (Figures 6b, c). The Kuroshio thus likely had a weak
533 or even no effect on the renewal of oxygen to the sedimentary environment during the
534 last glacial period. More recently, lower hydrothermal total Hg concentration during
535 20 ka - 9.6 ka, associated with reduced intensity and/or variation in flow path of KC,
536 relative to that of Holocene recorded in core KX12 - 3 (1423 water depth) (Lim et al.,
537 2017), further validates our inference.

538 On the other hand, the gradually increased alkenone-derived SST and abundance
539 of *P.obliquiloculata* (Figures 6d and 6e) from 15 ka onwards indicates an intensified
540 Kuroshio Current. At present, mooring and float observations revealed that the KC

541 penetrates to 1200 m isobath in the East China Sea (Andres et al., 2015). However, as
542 mentioned above, the effect of Kuroshio on the sedimentary oxygenation was likely
543 very limited during the glacial period and only gradually increasing throughout the
544 last glacial termination. Therefore, while its effect on our observed deglacial variation
545 in oxygenation may provide a slowly changing background condition in vertical
546 mixing effects on the sedimentary oxygenation in the OT, it cannot account for the
547 first order, rapid oxygenation changes, including indications for millennial-scale
548 variations, that we observe between 18 ka and 9 ka.

549 Better oxygenated sedimentary conditions since 8.5 ka coincided with intensified
550 Kuroshio (Li et al., 2005; Shi et al., 2014), as indicated by rapidly increased SST and
551 *P. obliquiloculata* abundance in core CSH1 (Figures 6d and 6e) and *C.hyalinea*
552 abundance in core E017 (Figure 6i). Re-entrance of the Kuroshio into the OT (Shi et
553 al., 2014) with rising eustatic sea level likely enhanced the vertical mixing and
554 exchange between bottom and surface waters, ventilating the deep water in the OT.
555 Previous comparative studies based on epibenthic $\delta^{13}\text{C}$ values indicated
556 well-ventilated deep water feeding both inside the OT and outside off the Ryukyu
557 Islands during the Holocene (Kubota et al., 2015; Wahyudi and Minagawa, 1997). In
558 summary, enhanced sedimentary oxygenation regime observed in the OT during the
559 Holocene is mainly related to the intensified Kuroshio, while the effect of the
560 Kuroshio on OT oxygenation was limited before 15 ka.

561 **6.2.4. Effects of GNPIW on sedimentary oxygenation**

562 Relatively stronger oxygenated Glacial North Pacific Intermediate Water
563 (GNPIW), coined by (Matsumoto et al., 2002), has been widely documented in the
564 Bering Sea (Itaki et al., 2012; Kim et al., 2011; Rella et al., 2012), the Okhotsk Sea
565 (Itaki et al., 2008; Okazaki et al., 2014; Okazaki et al., 2006; Wu et al., 2014), off east
566 Japan (Shibahara et al., 2007), the eastern North Pacific (Cartapanis et al., 2011;
567 Ohkushi et al., 2013) and western subarctic Pacific (Keigwin, 1998; Matsumoto et al.,
568 2002). The intensified formation of GNPIW due to the displacement of source region
569 to the Bering Sea was proposed by Ohkushi et al. (2003) and then is confirmed by
570 Horikawa et al. (2010). Under such conditions, the invasion of well-ventilated

571 GNPIW into the OT through the Kerama Gap would have replenished the water
572 column oxygen in the OT, although the penetration depth of GNPIW remains under
573 debate (Jaccard and Galbraith, 2013; Okazaki et al., 2010; Rae et al., 2014). Both a
574 gradual decrease in excess U concentration and an increase in Mo/Mn ratio during the
575 last glacial period (25 ka-50 ka) validate such inference, suggesting pronounced
576 effects of intensified NPIW formation in the OT.

577 During HS1, a stronger formation of GNPIW was supported by proxy studies
578 and numerical simulations. For example, on the basis of paired benthic-planktic (B-P)
579 ¹⁴C data, enhanced penetration of NPIW into a much deeper water depth during HS1
580 relative to the Holocene has been revealed in several studies (Max et al., 2014;
581 Okazaki et al., 2010; Sagawa and Ikehara, 2008), which was also simulated by several
582 models (Chikamoto et al., 2012; Gong et al., 2019; Okazaki et al., 2010). On the other
583 hand, increased intermediate water temperature in the subtropical Pacific recorded in
584 core GH08-2004 (1166 m water depth) (Kubota et al., 2015) and young deep water
585 observed in the northern South China Sea during HS1 (Wan and Jian, 2014) along
586 downstream region of NPIW are also related to intensified NPIW formation.
587 Furthermore, the pathway of GNPIW from numerical model simulations (Zheng et al.,
588 2016) was similar to modern observations (You, 2003). Thus, all these evidence imply
589 a persistent, cause and effect relation between GNPIW ventilation, the intermediate
590 and deep water oxygen concentration in the OT and sediment redox state during HS1.
591 In addition, our RSEs data also suggested a similarly enhanced ventilation in HS2
592 (Figures 6b and 6c) that is also attributed to intensified GNPIW.

593 Hypoxic conditions during the B/A have been also widely observed in the mid-
594 and high-latitude North Pacific (Jaccard and Galbraith, 2012; Praetorius et al., 2015).
595 Our data of excess U concentration and Mo/Mn ratio recorded in core CSH1 (Figures
596 6b and 6c), together with enhanced denitrification and *B.aculeata* abundance (Figures
597 6f and 6h), further reveal the expansion of oxygen-depletion at mid-depth waters
598 down to the subtropical NW Pacific during the late deglacial period. Based on high
599 relative abundances of radiolarian species, indicators of upper intermediate water
600 ventilation in core PC-23A, Itaki et al. (2012) suggested that a presence of

601 well-ventilated waters was limited to the upper intermediate layer (200 m–500 m) in
602 the Bering Sea during warm periods, such as the B/A and Preboreal. Higher B-P
603 foraminiferal ^{14}C ages, together with increased temperature and salinity at
604 intermediate waters recorded in core GH02-1030 (off East Japan) supported a
605 weakened formation of NPIW during the B/A (Sagawa and Ikehara, 2008). These
606 lines of evidence indicate that the boundary between GNPIW and North Pacific Deep
607 Water shoaled during the B/A, in comparison to HS1. Based on a comparison of two
608 benthic foraminiferal oxygen and carbon isotope records from off northern Japan and
609 the southern Ryukyu Island, Kubota et al. (2015) found a stronger influence of Pacific
610 Deep Water on intermediate-water temperature and ventilation at their southern than
611 the northern locations, though both sites are located at similar water depths (1166 m
612 and 1212 m for cores GH08-2004 and GH02-1030, respectively). Higher excess U
613 concentration and low Mo/Mn ratio in our core CSH1 during the B/A and Preboreal
614 suggest reduced sedimentary oxygenation, consistent with reduced ventilation of
615 GNPIW, contributing to the subsurface water deoxygenation in the OT.

616 During the YD, Mo/Mn ratio and excess U show a slightly decreased oxygen
617 condition in the northern OT. By contrast, benthic foraminiferal $\delta^{18}\text{O}$ and $\delta^{13}\text{C}$ values
618 in a sediment core collected from the Oyashio region suggested a strengthened
619 formation and ventilation of GNPIW during the YD (Ohkushi et al., 2016). This
620 pattern possibly indicates a time-dependent, varying contribution of distal GNPIW to
621 the deglacial OT oxygenation history, and we presume a more pronounced
622 contribution of organic matter degradation due to high export productivity during this
623 period, as suggested by increasing CaCO_3 content.

624 **6.3. Subtropical North Pacific ventilation links to North Atlantic Climate**

625 One of the characteristics climate features in the Northern Hemisphere, in
626 particular the North Atlantic is millennial-scale oscillations during the glacial and
627 deglacial periods. These abrupt climatic events have been widely thought to be related
628 to varying strength of Atlantic Meridional Overturning Circulation (AMOC)
629 (Lynch-Stieglitz, 2017). One of dynamic proxies of ocean circulation, $^{231}\text{Pa}/^{230}\text{Th}$
630 reveals that severe weakening of AMOC only existed during Heinrich stadials due to

631 increased freshwater discharges into the North Atlantic (Böhm et al., 2015; McManus
632 et al., 2004). On the other hand, several mechanisms, such as sudden termination of
633 freshwater input (Liu et al., 2009), atmospheric CO₂ concentration (Zhang et al.,
634 2017), enhanced advection of salt (Barker et al., 2010) and changes in background
635 climate (Knorr and Lohmann, 2007) were proposed to explain the reinvigoration of
636 AMOC during the B/A.

637 Our RSEs data in the Northern OT and epibenthic $\delta^{13}\text{C}$ in the Bering Sea
638 (Figures 7a-c) both show a substantial millennial variability in intermediate water
639 ventilation in the subtropical North Pacific. Notably, enhanced ventilation during HS1
640 and HS2 and oxygen-poor condition during the B/A respectively correspond to the
641 collapse and resumption of AMOC (Figure 7d). Such out-of-phase millennial-scale
642 pattern is consistent with the results of various modeling simulations (Chikamoto et
643 al., 2012; Menviel et al., 2014; Okazaki et al., 2010; Saenko et al., 2004), although
644 these models had different boundary conditions and causes for the observed effects in
645 GNPIW formation, and ventilation ages derived from B-P ^{14}C (Freeman et al., 2015;
646 Max et al., 2014; Okazaki et al., 2012). These lines of evidence confirm a persistent
647 link between the ventilation of North Pacific and the North Atlantic climate
648 (Lohmann et al., 2019). Such links have also been corroborated by proxy data and
649 modeling experiment between AMOC and East Asian monsoon during the 8.2 ka
650 event (Liu et al., 2013), the Holocene (Wang et al., 2005) and 34 ka–60 ka (Sun et al.,
651 2012). The mechanism linking East Asia with North Atlantic has been attributed to an
652 atmospheric teleconnection, such as the position and strength of Westerly Jet and
653 Mongolia-Siberian High (Porter and Zhisheng, 1995). However, the mechanism
654 behind such out-of-phase pattern between the ventilation in the subtropical North
655 Pacific and the North Atlantic deep water formation remains unclear.

656 Increased NPIW formation during HS1 may have been caused by enhanced
657 salinity-driven vertical mixing through higher meridional water mass transport from
658 the subtropical Pacific. Previous studies have proposed that intermediate water
659 formation in the North Pacific hinged on a basin-wide increase in sea surface salinity
660 driven by changes in strength of the summer EAM and the moisture transport from

661 the Atlantic to the Pacific (Emile-Geay et al., 2003). Several modeling studies found
662 that freshwater forcing in the North Atlantic could cause a widespread surface
663 salinification in the subtropical Pacific Ocean (Menviel et al., 2014; Okazaki et al.,
664 2010; Saenko et al., 2004). This idea has been tested by proxy data (Rodríguez-Sanz
665 et al., 2013; Sagawa and Ikehara, 2008), which indicated a weakened summer EAM
666 and reduced transport of moisture from Atlantic to Pacific through Panama Isthmus
667 owing to the southward displacement of Intertropical Convergence Zone caused by a
668 weakening of AMOC. Along with this process, as predicted through a general
669 circulation modeling, a strengthened Pacific Meridional Overturning Circulation
670 would have transported more warm and salty subtropical water into the high-latitude
671 North Pacific (Okazaki et al., 2010). In accordance with comprehensive Mg/Ca
672 ratio-based salinity reconstructions, however, Riethdorf et al. (2013) found no clear
673 evidence for such higher salinity patterns in the subarctic northwest Pacific during
674 HS1.

675 On the other hand, a weakened AMOC would deepen the wintertime Aleutian
676 Low based on modern observations (Okumura et al., 2009), which is closely related to
677 the sea ice formation in the marginal seas of the subarctic Pacific (Cavalieri and
678 Parkinson, 1987). Once stronger Aleutian Low, intense brine rejection due to sea ice
679 expansion, would have enhanced the NPIW formation. Recently our
680 modeling-derived evidence confirms that enhanced sea ice coverage occurred in the
681 southern Okhotsk Sea and off East Kamchatka Peninsula during HS1 (Gong et al.,
682 2019). In addition, stronger advection of low-salinity water via the Alaskan Stream to
683 the subarctic NW Pacific was probably enhanced during HS1, related to a shift of the
684 Aleutian Low pressure system over the North Pacific, which could also increase sea
685 ice formation, brine rejection and thereafter intermediate water ventilation (Riethdorf
686 et al., 2013).

687 During the late deglaciation, ameliorating global climate conditions, such as
688 warming Northern Hemisphere, and a strengthened Asian summer monsoon, are a
689 result of changes in insolation forcing, greenhouse gases concentrations, and variable
690 strengths of the AMOC (Clark et al., 2012; Liu et al., 2009). During the B/A, a

691 decrease in sea ice extent and duration, as well as reduced advection of Alaska Stream
692 waters were indicated by combined reconstructions of SST and mixed layer
693 temperatures from the subarctic Pacific (Riethdorf et al., 2013). At that time, the
694 rising eustatic sea level (Spratt and Lisiecki, 2016) would have supported the
695 intrusion of Alaska Stream into the Bering Sea by deepening and opening glacial
696 closed straits of the Aleutian Islands chain, while reducing the advection of the Alaska
697 Stream to the subarctic Pacific gyre (Riethdorf et al., 2013). In this scenario, saltier
698 and more stratified surface water conditions would have inhibited brine rejection and
699 subsequent formation and ventilation of NPIW (Lam et al., 2013), leading to a
700 reorganization of the Pacific water mass, closely coupled to the collapse and
701 resumption modes of the AMOC during these two intervals.

702 **6.4 Increased storage of CO₂ at mid-depth water in the North Pacific at the B/A**

703 One of the striking features of RSEs data is higher Mo/Mn ratio and excess U
704 concentration at the B/A, supporting an expansion of Oxygen Minimum Zone in the
705 North Pacific (Galbraith and Jaccard, 2015; Jaccard and Galbraith, 2012; Moffitt et al.,
706 2015) and coinciding with the termination of atmospheric CO₂ concentration rise
707 (Marcott et al., 2014) (Figure 7e). As described above, it can be related to the
708 upwelling of nutrient- and CO₂-rich Pacific Deep Water due to resumption of AMOC
709 and enhanced export production. Although here we are unable to distinguish these
710 two reasons from each other, boron isotope data measured on surface-dwelling
711 foraminifera in core MD01-2416 situated in the western subarctic North Pacific did
712 reveal a decrease in near-surface pH and an increase in pCO₂ at this time (Gray et al.,
713 2018). That is to say, subarctic North Pacific is a source of relatively high
714 atmospheric CO₂ concentration at the B/A. Here we cannot conclude that the same
715 processes could have occurred in the subtropical North Pacific due to the lack of
716 well-known drivers to draw out of the old carbon in the deep sea into the atmosphere.
717 However, an expansion of oxygen-depletion zone in the entire North Pacific suggest
718 an increase in respired carbon storage at intermediate-depth in the subtropical North
719 Pacific, which likely stalls the rise of atmospheric CO₂. Our results support the
720 findings by Galbraith et al. (2007) and are consistent with the hypothesis of deglacial

721 flushing of respired carbon dioxide from an isolated, deep ocean reservoir (Marchitto
722 et al., 2007; Sigman and Boyle, 2000). Given the sizeable volume of the North Pacific,
723 potentially, once the respired carbon could be emitted to the atmosphere in stages,
724 which would play an important role in propelling the Earth out of the last ice age
725 (Jaccard and Galbraith, 2018).

726 **7. Conclusions**

727 Our geochemical results of sediment core CSH1 revealed substantial changes in
728 intermediate water redox conditions in the northern Okinawa Trough over the last 50
729 ka on orbital and millennial timescales. Enhanced sedimentary oxygenation mainly
730 occurred during cold intervals, such as the last glacial period, Heinrich stadials 1 and
731 2, and during the middle and late Holocene, while diminished sedimentary
732 oxygenation prevailed during the Bölling-Alleröd and Preboreal. The sedimentary
733 oxygenation variability presented here provides key evidence for the substantial
734 impact of ventilation of NPIW on the sedimentary oxygenation in the subtropical
735 North Pacific and shows out-of-phase pattern with North Atlantic Climate during the
736 last deglaciation. The linkage is attributable to the disruption of NPIW formation
737 caused by climate changes in the North Atlantic, which is transferred to the North
738 Pacific via atmospheric and oceanic teleconnections. We also suggest an expansion of
739 oxygen-depleted zone and accumulation of respired carbon at the mid-depth waters of
740 the North Pacific during the B/A, coinciding with the termination of atmospheric CO₂
741 rise. A step-wise injection of such respired carbon into the atmosphere, the mechanism
742 likely to propel the Earth out of glacial climate, would be helpful to maintain high
743 atmospheric CO₂ levels during the deglaciation.

744

745 **Data availability.** All raw data are available to all interested researchers upon request.

746

747 **Author Contributions.** J.J.Z. and X.F.S. conceived the study. A.M.Z. performed
748 geochemical analyses of bulk sediments. J.J.Z., X.F.S. K.S. and X.G. led the write up
749 of the manuscript. All other authors provided comments on the manuscript and
750 contributed to the final version of the manuscript.

751

752 **Competing interests:** The authors declare no competing interests.

753

754 **Acknowledgements**

755 Financial support was provided by the National Program on Global Change and
756 Air-Sea Interaction (GASI-GEOGE-04), by the National Natural Science Foundation
757 of China (Grant Nos.: 41476056, 41876065, 41420104005, 41206059, and U1606401)
758 and by the Basic Scientific Fund for National Public Research Institutes of China
759 (No.2016Q09) and International Cooperative Projects in Polar Study (201613) and
760 Taishan Scholars Program of Shandong. This study is a contribution to the bilateral
761 Sino-German collaboration project (funding through BMBF grant 03F0704A –
762 SIGEPAX). XG, LLJ, GL, RT thank the bilateral Sino-German collaboration
763 NOPAWAC project (BMBF grant No. 03F0785A).LLJ and RT acknowledge financial
764 support through the national Helmholtz REKLIM Initiative. We would like to thank
765 the anonymous reviewers, who helped to improve the quality of this manuscript. The
766 data used in this study are available from the authors upon request
767 (zoujianjun@fio.org.cn).

768

769 **References**

770 Addison, J. A., Finney, B. P., Dean, W. E., Davies, M. H., Mix, A. C., Stoner, J. S., and Jaeger, J. M.:
771 Productivity and sedimentary $\delta^{15}\text{N}$ variability for the last 17,000 years along the northern Gulf of
772 Alaska continental slope, *Paleoceanography*, 27, PA1206, doi:1210.1029/2011PA002161, 2012.
773 Algeo, T. J.: Can marine anoxic events draw down the trace element inventory of seawater?, *Geology*,
774 32, 1057-1060, 2004.
775 Algeo, T. J. and Lyons, T. W.: Mo-total organic carbon covariation in modern anoxic marine
776 environments: Implications for analysis of paleoredox and paleohydrographic conditions,
777 *Paleoceanography*, 21, PA1016, doi: 1010.1029/2004pa001112, 2006.
778 Algeo, T. J. and Tribovillard, N.: Environmental analysis of paleoceanographic systems based on
779 molybdenum – uranium covariation, *Chemical Geology*, 268, 211-225, 2009.
780 Andres, M., Jan, S., Sanford, T. B., Mensah, V., Centurioni, L. R., and Book, J. W.: Mean structure and
781 variability of the Kuroshio from northeastern Taiwan to southwestern Japan, *Oceanography*, 26, 84–95,
782 2015.
783 Böhm, E., Lippold, J., Gutjahr, M., Frank, M., Blaser, P., Antz, B., Fohlmeister, J., Frank, N., Andersen,
784 M. B., and Deininger, M.: Strong and deep Atlantic meridional overturning circulation during the last
785 glacial cycle, *Nature*, 517, 73-76, 2015.

786 Barker, S., Knorr, G., Vautravers, M. J., Diz, P., and Skinner, L. C.: Extreme deepening of the Atlantic
787 overturning circulation during deglaciation, *Nature Geoscience*, 3, 567-571, 2010.

788 Bianchi, D., Dunne, J. P., Sarmiento, J. L., and Galbraith, E. D.: Data-based estimates of suboxia,
789 denitrification, and N₂O production in the ocean and their sensitivities to dissolved O₂, *Global*
790 *Biogeochemical Cycles*, 26, doi:10.1029/2011gb004209, 2012.

791 Brewer, P. G. and Peltzer, E. T.: Ocean chemistry, ocean warming, and emerging hypoxia: Commentary,
792 *Journal of Geophysical Research: Oceans*, 121, 3659-3667, 2016.

793 Burdige, D. J.: The biogeochemistry of manganese and iron reduction in marine sediments,
794 *Earth-Science Reviews*, 35, 249-284, 1993.

795 Cannariato, K. G. and Kennett, J. P.: Climatically related millennial-scale fluctuations in strength of
796 California margin oxygen-minimum zone during the past 60 k.y, *Geology*, 27, 975-978, 1999.

797 Cartapanis, O., Tachikawa, K., and Bard, E.: Northeastern Pacific oxygen minimum zone variability
798 over the past 70 kyr: Impact of biological production and oceanic ventilation, *Paleoceanography*, 26,
799 PA4208, doi: 4210.1029/2011PA002126, 2011.

800 Cavalieri, D. J. and Parkinson, C. L.: On the relationship between atmospheric circulation and the
801 fluctuations in the sea ice extents of the bering and okhotsk seas, *Journal of Geophysical*
802 *Research-Oceans*, 92, 7141-7162, 1987.

803 Chang, A. S., Pedersen, T. F., and Hendy, I. L.: Effects of productivity, glaciation, and ventilation on
804 late Quaternary sedimentary redox and trace element accumulation on the Vancouver Island margin,
805 western Canada, *Paleoceanography*, 29, doi: 10.1002/2013PA002581, 2014.

806 Chang, Y.-P., Chen, M.-T., Yokoyama, Y., Matsuzaki, H., Thompson, W. G., Kao, S.-J., and Kawahata,
807 H.: Monsoon hydrography and productivity changes in the East China Sea during the past 100,000
808 years: Okinawa Trough evidence (MD012404), *Paleoceanography*, 24, PA3208, doi:
809 3210.1029/2007PA001577, 2009.

810 Chen, J., Zhang, D., Zhang, W., and Li, T.: The paleoclimatic change since the last galciation in the
811 north of Okinawa Trough based on the spore-pollen records, *Acta Oceanologica Sinica*, 28, 85-91(in
812 Chinese with English Abstract), 2006.

813 Cheng, H., Edwards, R. L., Sinha, A., Spötl, C., Yi, L., Chen, S., Kelly, M., Kathayat, G., Wang, X., Li,
814 X., Kong, X., Wang, Y., Ning, Y., and Zhang, H.: The Asian monsoon over the past 640,000 years and
815 ice age terminations, *Nature*, 534, 640-646, 2016.

816 Cheng, H., Edwards, R. L., Southon, J., Matsumoto, K., Feinberg, J. M., Sinha, A., Zhou, W., Li, H., Li,
817 X., Xu, Y., Chen, S., Tan, M., Wang, Q., Wang, Y., and Ning, Y.: Atmospheric 14C/12C changes during
818 the last glacial period from Hulu Cave, *Science*, 362, 1293-1297, 2018.

819 Chikamoto, M. O., Menviel, L., Abe-Ouchi, A., Ohgaito, R., Timmermann, A., Okazaki, Y., Harada, N.,
820 Oka, A., and Mouchet, A.: Variability in North Pacific intermediate and deep water ventilation during
821 Heinrich events in two coupled climate models, *Deep Sea Research Part II: Topical Studies in*
822 *Oceanography*, 61-64, 114-126, 2012.

823 Clark, P. U., Shakun, J. D., Baker, P. A., Bartlein, P. J., Brewer, S., Brook, E., Carlson, A. E., Cheng, H.,
824 Kaufman, D. S., Liu, Z., Marchitto, T. M., Mix, A. C., Morrill, C., Otto-Bliesner, B. L., Pahnke, K.,
825 Russell, J. M., Whitlock, C., Adkins, J. F., Blois, J. L., Clark, J., Colman, S. M., Curry, W. B., Flower,
826 B. P., He, F., Johnson, T. C., Lynch-Stieglitz, J., Markgraf, V., McManus, J., Mitrovica, J. X., Moreno, P.
827 I., and Williams, J. W.: Global climate evolution during the last deglaciation, *Proceedings of the*
828 *National Academy of Sciences of the United States of America*, 109, E1134-E1142, 2012.

829 Clemens, S. C., Holbourn, A., Kubota, Y., Lee, K. E., Liu, Z., Chen, G., Nelson, A., and Fox-Kemper,

830 B.: Precession-band variance missing from East Asian monsoon runoff, *Nature Communications*, 9,
831 3364, doi: 3310.1038/s41467-41018-05814-41460, 2018.

832 Crusius, J., Calvert, S., Pedersen, T., and Sage, D.: Rhenium and molybdenum enrichments in
833 sediments as indicators of oxic, suboxic and sulfidic conditions of deposition, *Earth and Planetary*
834 *Science Letters*, 145, 65-78, 1996.

835 Crusius, J., Pedersen, T. F., Kienast, S., Keigwin, L., and Labeyrie, L.: Influence of northwest Pacific
836 productivity on North Pacific Intermediate Water oxygen concentrations during the Boiling-Allerod
837 interval (14.7-12.9 ka), *Geology*, 32, 633-636, 2004.

838 Dahl, T. W., Anbar, A. D., Gordon, G. W., Rosing, M. T., Frei, R., and Canfield, D. E.: The behavior of
839 molybdenum and its isotopes across the chemocline and in the sediments of sulfidic Lake Cadagno,
840 Switzerland, *Geochimica et Cosmochimica Acta*, 74, 144-163, 2010.

841 Dean, W. E., Gardner, J. V., and Piper, D. Z.: Inorganic geochemical indicators of glacial-interglacial
842 changes in productivity and anoxia on the California continental margin, *Geochimica et Cosmochimica*
843 *Acta*, 61, 4507-4518, 1997.

844 Delcroix, T. and Murtugudde, R.: Sea surface salinity changes in the East China Sea during 1997–2001:
845 Influence of the Yangtze River, *Journal of Geophysical Research: Oceans*, 107, 8008,
846 doi:8010.1029/2001JC000893, 2002.

847 Dou, Y., Yang, S., Li, C., Shi, X., Liu, J., and Bi, L.: Deepwater redox changes in the southern Okinawa
848 Trough since the last glacial maximum, *Progress in Oceanography*, 135, 77-90, 2015.

849 Emile-Geay, J., Cane, M. A., Naik, N., Seager, R., Clement, A. C., and van Geen, A.: Warren revisited:
850 Atmospheric freshwater fluxes and “Why is no deep water formed in the North Pacific”, *Journal of*
851 *Geophysical Research: Oceans*, 108, doi:10.1029/2001JC001058, 2003.

852 Freeman, E., Skinner, L. C., Tisserand, A., Dokken, T., Timmermann, A., Menviel, L., and Friedrich, T.:
853 An Atlantic–Pacific ventilation seesaw across the last deglaciation, *Earth and Planetary Science Letters*,
854 424, 237-244, 2015.

855 Galbraith, E. D. and Jaccard, S. L.: Deglacial weakening of the oceanic soft tissue pump: global
856 constraints from sedimentary nitrogen isotopes and oxygenation proxies, *Quaternary Science Reviews*,
857 109, 38-48, 2015.

858 Galbraith, E. D., Jaccard, S. L., Pedersen, T. F., Sigman, D. M., Haug, G. H., Cook, M., Southon, J. R.,
859 and Francois, R.: Carbon dioxide release from the North Pacific abyss during the last deglaciation,
860 *Nature*, 449, 890-893, 2007.

861 Galbraith, E. D., Kienast, M., Pedersen, T. F., and Calvert, S. E.: Glacial-interglacial modulation of the
862 marine nitrogen cycle by high-latitude O₂ supply to the global thermocline, *Paleoceanography*, 19,
863 PA4007, doi:4010.1029/2003PA001000, 2004.

864 Ge, S., Shi, X., Wu, Y., Lee, T., Xiong, Y., and Saito, Y.: Rock magnetic property of gravity core CSH1
865 from the northern Okinawa Trough and the effect of early diagenesis, *Acta Oceanologica Sinica*, 26,
866 54-65, 2007.

867 Gong, X., Lembke-Jene, L., Lohmann, G., Knorr, G., Tiedemann, R., Zou, J. J., and Shi, X. F.:
868 Enhanced North Pacific deep-ocean stratification by stronger intermediate water formation during
869 Heinrich Stadial 1, *Nature Communications*, 10, 656, doi:610.1038/s41467-41019-08606-41462, 2019.

870 Gray, W. R., Rae, J. W. B., Wills, R. C. J., Shevenell, A. E., Taylor, B., Burke, A., Foster, G. L., and
871 Lear, C. H.: Deglacial upwelling, productivity and CO₂ outgassing in the North Pacific Ocean, *Nature*
872 *Geoscience*, 11, 340-344, 2018.

873 Helz, G. R., Miller, C. V., Charnock, J. M., Mosselmans, J. F. W., Patrick, R. A. D., Garner, C. D., and

874 Vaughan, D. J.: Mechanism of molybdenum removal from the sea and its concentration in black shales:
875 EXAFS evidence, *Geochimica et Cosmochimica Acta*, 60, 3631-3642, 1996.

876 Hofmann, A. F., Peltzer, E. T., Walz, P. M., and Brewer, P. G.: Hypoxia by degrees: Establishing
877 definitions for a changing ocean, *Deep Sea Research Part I: Oceanographic Research Papers*, 58,
878 1212-1226, 2011.

879 Hoogakker, B. A. A., Elderfield, H., Schmiedl, G., McCave, I. N., and Rickaby, R. E. M.:
880 Glacial–interglacial changes in bottom-water oxygen content on the Portuguese margin, *Nature*
881 *Geoscience*, 8, 40-43, 2015.

882 Horikawa, K., Asahara, Y., Yamamoto, K., and Okazaki, Y.: Intermediate water formation in the Bering
883 Sea during glacial periods: Evidence from neodymium isotope ratios, *Geology*, 38, 435-438, 2010.

884 Ichikawa, H. and Beardsley, R. C.: The Current System in the Yellow and East China Seas, *Journal of*
885 *Oceanography*, 58, 77-92, 2002.

886 Itaki, T., Khim, B. K., and Ikehara, K.: Last glacial-Holocene water structure in the southwestern
887 Okhotsk Sea inferred from radiolarian assemblages, *Marine Micropaleontology*, 67, 191-215, 2008.

888 Itaki, T., Kim, S., Rella, S. F., Uchida, M., Tada, R., and Khim, B. K.: Millennial-scale variations of
889 late Pleistocene radiolarian assemblages in the Bering Sea related to environments in shallow and deep
890 waters, *Deep-Sea Research Part II-Topical Studies in Oceanography*, 61-64, 127-144, 2012.

891 Ivanochko, T. S. and Pedersen, T. F.: Determining the influences of Late Quaternary ventilation and
892 productivity variations on Santa Barbara Basin sedimentary oxygenation: a multi-proxy approach,
893 *Quaternary Science Reviews*, 23, 467-480, 2004.

894 Jaccard, S. L. and Galbraith, E. D.: Direct ventilation of the North Pacific did not reach the deep ocean
895 during the last deglaciation, *Geophysical Research Letters*, 40, 199-203, 2013.

896 Jaccard, S. L. and Galbraith, E. D.: Large climate-driven changes of oceanic oxygen concentrations
897 during the last deglaciation, *Nature Geoscience*, 5, 151-156, 2012.

898 Jaccard, S. L. and Galbraith, E. D.: Push from the Pacific, *Nature Geoscience*, 11, 299-300, 2018.

899 Jaccard, S. L., Galbraith, E. D., Martínez-García, A., and Anderson, R. F.: Covariation of deep
900 Southern Ocean oxygenation and atmospheric CO₂ through the last ice age, *Nature*, 530, 207-210,
901 2016.

902 Jaccard, S. L., Galbraith, E. D., Sigman, D. M., Haug, G. H., Francois, R., Pedersen, T. F., Dulski, P.,
903 and Thierstein, H. R.: Subarctic Pacific evidence for a glacial deepening of the oceanic respired carbon
904 pool, *Earth and Planetary Science Letters*, 277, 156-165, 2009.

905 Jian, Z. M., Chen, R. H., and Li, B. H.: Deep-sea benthic foraminiferal record of the paleoceanography
906 in the southern Okinawa trough over the last 20000 years, *Science in China Series D-Earth Sciences*,
907 39, 551-560, 1996.

908 Kao, S. J., Horng, C. S., Hsu, S. C., Wei, K. Y., Chen, J., and Lin, Y. S.: Enhanced deepwater
909 circulation and shift of sedimentary organic matter oxidation pathway in the Okinawa Trough since the
910 Holocene, *Geophysical Research Letters*, 32, L15609, doi:15610.11029/12005GL023139, 2005.

911 Kao, S. J., Liu, K. K., Hsu, S. C., Chang, Y. P., and Dai, M. H.: North Pacific-wide spreading of
912 isotopically heavy nitrogen during the last deglaciation: Evidence from the western Pacific,
913 *Biogeosciences*, 5, 1641-1650, 2008.

914 Kao, S. J., Wu, C.-R., Hsin, Y.-C., and Dai, M.: Effects of sea level change on the upstream Kuroshio
915 Current through the Okinawa Trough, *Geophysical Research Letters*, 33, L16604,
916 doi:16610.11029/12006gl026822, 2006.

917 Keigwin, L. D.: Glacial-age hydrography of the far northwest Pacific Ocean, *Paleoceanography*, 13,

918 323-339, 1998.

919 Kim, S., Khim, B. K., Uchida, M., Itaki, T., and Tada, R.: Millennial-scale paleoceanographic events
920 and implication for the intermediate-water ventilation in the northern slope area of the Bering Sea
921 during the last 71 kyrs, *Global and Planetary Change*, 79, 89-98, 2011.

922 Klinkhammer, G. P. and Palmer, M. R.: Uranium in the oceans: Where it goes and why, *Geochimica et*
923 *Cosmochimica Acta*, 55, 1799-1806, 1991.

924 Knorr, G. and Lohmann, G.: Rapid transitions in the Atlantic thermohaline circulation triggered by
925 global warming and meltwater during the last deglaciation, *Geochemistry, Geophysics, Geosystems*, 8,
926 DOI: 10.1029/2007gc001604, 2007.

927 Kohfeld, K. E. and Chase, Z.: Controls on deglacial changes in biogenic fluxes in the North Pacific
928 Ocean, *Quaternary Science Reviews*, 30, 3350-3363, 2011.

929 Kubota, Y., Kimoto, K., Itaki, T., Yokoyama, Y., Miyairi, Y., and Matsuzaki, H.: Bottom water
930 variability in the subtropical northwestern Pacific from 26 kyr BP to present based on Mg/Ca and stable
931 carbon and oxygen isotopes of benthic foraminifera, *Climate of the Past*, 11, 803-824, 2015.

932 Kubota, Y., Kimoto, K., Tada, R., Oda, H., Yokoyama, Y., and Matsuzaki, H.: Variations of East Asian
933 summer monsoon since the last deglaciation based on Mg/Ca and oxygen isotope of planktic
934 foraminifera in the northern East China Sea, *Paleoceanography*, 25, PA4205,
935 doi:4210.1029/2009pa001891, 2010.

936 Lam, P. J., Robinson, L. F., Blusztajn, J., Li, C., Cook, M. S., McManus, J. F., and Keigwin, L. D.:
937 Transient stratification as the cause of the North Pacific productivity spike during deglaciation, *Nature*
938 *Geosci*, 6, 622-626, 2013.

939 Lee, K. E., Lee, H. J., Park, J.-H., Chang, Y.-P., Ikehara, K., Itaki, T., and Kwon, H. K.: Stability of the
940 Kuroshio path with respect to glacial sea level lowering, *Geophysical Research Letters*, 40, 392–396,
941 doi:310.1002/grl.50102, 2013.

942 Lembke-Jene, L., Tiedemann, R., Nürnberg, D., Kokfelt, U., Kozdon, R., Max, L., Röhl, U., and
943 Gorbarenko, S. A.: Deglacial variability in Okhotsk Sea Intermediate Water ventilation and
944 biogeochemistry: Implications for North Pacific nutrient supply and productivity, *Quaternary Science*
945 *Reviews*, 160, 116-137, 2017.

946 Li, D., Zheng, L.-W., Jaccard, S. L., Fang, T.-H., Paytan, A., Zheng, X., Chang, Y.-P., and Kao, S.-J.:
947 Millennial-scale ocean dynamics controlled export productivity in the subtropical North Pacific,
948 *Geology*, 45, 651-654, 2017.

949 Li, T. G., Xiang, R., Sun, R. T., and Cao, Q. Y.: Benthic foraminifera and bottom water evolution in the
950 middle-southern Okinawa Trough during the last 18 ka, *Science in China Series D-Earth Sciences*, 48,
951 805-814, 2005.

952 Li, Y. H. and Schoonmaker, J. E.: Chemical Composition and Mineralogy of Marine Sediments. In:
953 *Treatise on Geochemistry (Second Edition)*, Turekian, K. K. (Ed.), Elsevier, Oxford, 2014.

954 Lim, D., Kim, J., Xu, Z., Jeong, K., and Jung, H.: New evidence for Kuroshio inflow and deepwater
955 circulation in the Okinawa Trough, East China Sea: Sedimentary mercury variations over the last
956 20 kyr, *Paleoceanography*, 32, 571-579, 2017.

957 Liu, Y. H., Henderson, G. M., Hu, C. Y., Mason, A. J., Charnley, N., Johnson, K. R., and Xie, S. C.:
958 Links between the East Asian monsoon and North Atlantic climate during the 8,200 year event, *Nature*
959 *Geosci*, 6, 117-120, 2013.

960 Liu, Z., Otto-Bliesner, B. L., He, F., Brady, E. C., Tomas, R., Clark, P. U., Carlson, A. E.,
961 Lynch-Stieglitz, J., Curry, W., Brook, E., Erickson, D., Jacob, R., Kutzbach, J., and Cheng, J.: Transient

962 Simulation of Last Deglaciation with a New Mechanism for Bølling-Allerød Warming, *Science*, 325,
963 310-314, 2009.

964 Lynch-Stieglitz, J.: The Atlantic Meridional Overturning Circulation and Abrupt Climate Change,
965 *Annual Review of Marine Science*, 9, 83-104, 2017.

966 Lyons, T. W., Anbar, A. D., Severmann, S., Scott, C., and Gill, B. C.: Tracking Euxinia in the Ancient
967 Ocean: A Multiproxy Perspective and Proterozoic Case Study, *Annual Review of Earth and Planetary*
968 *Sciences*, 37, 507-534, 2009.

969 Machida, H.: The stratigraphy, chronology and distribution of distal marker-tephras in and around
970 Japan, *Global and Planetary Change*, 21, 71-94, 1999.

971 Maithani, P. B. and Srinivasan, S.: Felsic Volcanic Rocks, a Potential Source of Uranium - An Indian
972 Overview, *Energy Procedia*, 7, 163-168, 2011.

973 Marchitto, T. M., Lehman, S. J., Ortiz, J. D., Flückiger, J., and van Geen, A.: Marine Radiocarbon
974 Evidence for the Mechanism of Deglacial Atmospheric CO₂ Rise, *Science*, 316, 1456-1459, 2007.

975 Marcott, S. A., Bauska, T. K., Buizert, C., Steig, E. J., Rosen, J. L., Cuffey, K. M., Fudge, T. J.,
976 Severinghaus, J. P., Ahn, J., Kalk, M. L., McConnell, J. R., Sowers, T., Taylor, K. C., White, J. W. C.,
977 and Brook, E. J.: Centennial-scale changes in the global carbon cycle during the last deglaciation,
978 *Nature*, 514, 616-619, 2014.

979 Matsumoto, K., Oba, T., Lynch-Stieglitz, J., and Yamamoto, H.: Interior hydrography and circulation of
980 the glacial Pacific Ocean, *Quaternary Science Reviews*, 21, 1693-1704, 2002.

981 Max, L., Lembke-Jene, L., Riethdorf, J. R., Tiedemann, R., Nurnberg, D., Kuhn, H., and Mackensen,
982 A.: Pulses of enhanced North Pacific Intermediate Water ventilation from the Okhotsk Sea and Bering
983 Sea during the last deglaciation, *Climate of the Past*, 10, 591-605, 2014.

984 McManus, J., Berelson, W. M., Klinkhammer, G. P., Hammond, D. E., and Holm, C.: Authigenic
985 uranium: Relationship to oxygen penetration depth and organic carbon rain, *Geochimica et*
986 *Cosmochimica Acta*, 69, 95-108, 2005.

987 McManus, J. F., Francois, R., Gherardi, J. M., Keigwin, L. D., and Brown-Leger, S.: Collapse and rapid
988 resumption of Atlantic meridional circulation linked to deglacial climate changes, *Nature*, 428, 834-837,
989 2004.

990 Menviel, L., England, M. H., Meissner, K. J., Mouchet, A., and Yu, J.: Atlantic-Pacific seesaw and its
991 role in outgassing CO₂ during Heinrich events, *Paleoceanography*, 29, 58-70, 2014.

992 Moffitt, S. E., Moffitt, R. A., Sauthoff, W., Davis, C. V., Hewett, K., and Hill, T. M.: Paleoceanographic
993 Insights on Recent Oxygen Minimum Zone Expansion: Lessons for Modern Oceanography, *PLOS*
994 *ONE*, 10, e0115246, doi, 0115210.0111371/journal.pone.0115246, 2015.

995 Morford, J. L. and Emerson, S.: The geochemistry of redox sensitive trace metals in sediments,
996 *Geochimica et Cosmochimica Acta*, 63, 1735-1750, 1999.

997 Nakamura, H., Nishina, A., Liu, Z. J., Tanaka, F., Wimbush, M., and Park, J. H.: Intermediate and deep
998 water formation in the Okinawa Trough, *Journal of Geophysical Research-Oceans*, 118, 6881-6893,
999 2013.

1000 Nameroff, T. J., Balistrieri, L. S., and Murray, J. W.: Suboxic trace metal geochemistry in the Eastern
1001 Tropical North Pacific, *Geochimica et Cosmochimica Acta*, 66, 1139-1158, 2002.

1002 Nameroff, T. J., Calvert, S. E., and Murray, J. W.: Glacial-interglacial variability in the eastern tropical
1003 North Pacific oxygen minimum zone recorded by redox-sensitive trace metals, *Paleoceanography*, 19,
1004 PA1010, doi:10.1029/2003PA000912, 2004.

1005 Nishina, A., Nakamura, H., Park, J.-H., Hasegawa, D., Tanaka, Y., Seo, S., and Hibiya, T.: Deep

1006 ventilation in the Okinawa Trough induced by Kerama Gap overflow, *Journal of Geophysical Research:*
1007 *Oceans*, 121, 6092-6102, 2016.

1008 Ohkushi, K., Hara, N., Ikehara, M., Uchida, M., and Ahagon, N.: Intensification of North Pacific
1009 intermediate water ventilation during the Younger Dryas, *Geo-Mar Lett*, 36, 353-360, 2016.

1010 Ohkushi, K., Itaki, T., and Nemoto, N.: Last Glacial-Holocene change in intermediate-water ventilation
1011 in the Northwestern Pacific, *Quaternary Science Reviews*, 22, 1477-1484, 2003.

1012 Ohkushi, K., Kennett, J. P., Zeleski, C. M., Moffitt, S. E., Hill, T. M., Robert, C., Beaufort, L., and Behl,
1013 R. J.: Quantified intermediate water oxygenation history of the NE Pacific: A new benthic foraminiferal
1014 record from Santa Barbara basin, *Paleoceanography*, 28, 453-467, 2013.

1015 Okazaki, Y., Kimoto, K., Asahi, H., Sato, M., Nakamura, Y., and Harada, N.: Glacial to deglacial
1016 ventilation and productivity changes in the southern Okhotsk Sea, *Palaeogeography Palaeoclimatology*
1017 *Palaeoecology*, 395, 53-66, 2014.

1018 Okazaki, Y., Sagawa, T., Asahi, H., Horikawa, K., and Onodera, J.: Ventilation changes in the western
1019 North Pacific since the last glacial period, *Climate of the Past*, 8, 17-24, 2012.

1020 Okazaki, Y., Seki, O., Nakatsuka, T., Sakamoto, T., Ikehara, M., and Takahashi, K.: *Cycladophora*
1021 *davisiana* (Radiolaria) in the Okhotsk Sea: A key for reconstructing glacial ocean conditions, *Journal of*
1022 *Oceanography*, 62, 639-648, 2006.

1023 Okazaki, Y., Timmermann, A., Menviel, L., Harada, N., Abe-Ouchi, A., Chikamoto, M. O., Mouchet,
1024 A., and Asahi, H.: Deepwater Formation in the North Pacific During the Last Glacial Termination,
1025 *Science*, 329, 200-204, 2010.

1026 Okumura, Y. M., Deser, C., Hu, A., Timmermann, A., and Xie, S.-P.: North Pacific Climate Response to
1027 Freshwater Forcing in the Subarctic North Atlantic: Oceanic and Atmospheric Pathways, *Journal of*
1028 *Climate*, 22, 1424-1445, 2009.

1029 Porter, S. C. and Zhisheng, A.: Correlation between climate events in the North Atlantic and China
1030 during the last glaciation, *Nature*, 375, 305-308, 1995.

1031 Praetorius, S. K., Mix, A. C., Walczak, M. H., Wolhowe, M. D., Addison, J. A., and Prahl, F. G.: North
1032 Pacific deglacial hypoxic events linked to abrupt ocean warming, *Nature*, 527, 362-366, 2015.

1033 Qu, T. and Lukas, R.: The Bifurcation of the North Equatorial Current in the Pacific, *Journal of*
1034 *Physical Oceanography*, 33, 5-18, 2003.

1035 Rühlemann, C., Müller, P. J., and Schneider, R. R.: Organic Carbon and Carbonate as Paleoproductivity
1036 Proxies: Examples from High and Low Productivity Areas of the Tropical Atlantic. In: *Use of Proxies*
1037 *in Paleoceanography: Examples from the South Atlantic*, Fischer, G. and Wefer, G. (Eds.), Springer
1038 Berlin Heidelberg, Berlin, Heidelberg, 1999.

1039 Rae, J. W. B., Sarnthein, M., Foster, G. L., Ridgwell, A., Grootes, P. M., and Elliott, T.: Deep water
1040 formation in the North Pacific and deglacial CO₂ rise, *Paleoceanography*, 29, 645-667, 2014.

1041 Reimer, P. J., Bard, E., Bayliss, A., Beck, J. W., Blackwell, P. G., Bronk Ramsey, C., Buck, C. E.,
1042 Cheng, H., Edwards, R. L., Friedrich, M., Grootes, P. M., Guilderson, T. P., Haflidason, H., Hajdas, I.,
1043 Hatté, C., Heaton, T. J., Hoffmann, D. L., Hogg, A. G., Hughen, K. A., Kaiser, K. F., Kromer, B.,
1044 Manning, S. W., Niu, M., Reimer, R. W., Richards, D. A., Scott, E. M., Southon, J. R., Staff, R. A.,
1045 Turney, C. S. M., and van der Plicht, J.: IntCal13 and Marine13 Radiocarbon Age Calibration Curves
1046 0–50,000 Years cal BP, *Radiocarbon*, 55, 1869-1887, 2013.

1047 Rella, S. F., Tada, R., Nagashima, K., Ikehara, M., Itaki, T., Ohkushi, K., Sakamoto, T., Harada, N., and
1048 Uchida, M.: Abrupt changes of intermediate water properties on the northeastern slope of the Bering
1049 Sea during the last glacial and deglacial period, *Paleoceanography*, 27, PA3203,

1050 doi:3210.1029/2011pa002205, 2012.

1051 Riethdorf, J.-R., Max, L., Nuernberg, D., Lembke-Jene, L., and Tiedemann, R.: Deglacial development
1052 of (sub) sea surface temperature and salinity in the subarctic northwest Pacific: Implications for
1053 upper-ocean stratification, *Paleoceanography*, 28, doi:10.1002/palo.20014, 2013.

1054 Riethdorf, J.-R., Thibodeau, B., Ikehara, M., Nürnberg, D., Max, L., Tiedemann, R., and Yokoyama, Y.:
1055 Surface nitrate utilization in the Bering sea since 180ka BP: Insight from sedimentary nitrogen
1056 isotopes, *Deep Sea Research Part II: Topical Studies in Oceanography*, 125-126, 163-176, 2016.

1057 Rippert, N., Max, L., Mackensen, A., Cacho, I., Povea, P., and Tiedemann, R.: Alternating Influence of
1058 Northern Versus Southern-Sourced Water Masses on the Equatorial Pacific Subthermocline During the
1059 Past 240 ka, *Paleoceanography*, 32, 1256-1274, 2017.

1060 Rodríguez-Sanz, L., Mortyn, P. G., Herguera, J. C., and Zahn, R.: Hydrographic changes in the tropical
1061 and extratropical Pacific during the last deglaciation, *Paleoceanography*, 28, 529-538, 2013.

1062 Saenko, O. A., Schmittner, A., and Weaver, A. J.: The Atlantic-Pacific seesaw, *Journal of Climate*, 17,
1063 2033-2038, 2004.

1064 Sagawa, T. and Ikehara, K.: Intermediate water ventilation change in the subarctic northwest Pacific
1065 during the last deglaciation, *Geophysical Research Letters*, 35, 5, doi: 10.1029/2008gl035133, 2008.

1066 Scott, C. and Lyons, T. W.: Contrasting molybdenum cycling and isotopic properties in euxinic versus
1067 non-euxinic sediments and sedimentary rocks: Refining the paleoproxies, *Chemical Geology*, 324–325,
1068 19-27, 2012.

1069 Scott, C., Lyons, T. W., Bekker, A., Shen, Y., Poulton, S. W., Chu, X., and Anbar, A. D.: Tracing the
1070 stepwise oxygenation of the Proterozoic ocean, *Nature*, 452, 456-459, 2008.

1071 Shao, H., Yang, S., Cai, F., Li, C., Liang, J., Li, Q., Hyun, S., Kao, S.-J., Dou, Y., Hu, B., Dong, G., and
1072 Wang, F.: Sources and burial of organic carbon in the middle Okinawa Trough during late Quaternary
1073 paleoenvironmental change, *Deep Sea Research Part I: Oceanographic Research Papers*, 118, 46-56,
1074 2016.

1075 Shcherbina, A. Y., Talley, L. D., and Rudnick, D. L.: Direct observations of North Pacific ventilation:
1076 Brine rejection in the Okhotsk Sea, *Science*, 302, 1952-1955, 2003.

1077 Shi, X., Wu, Y., Zou, J., Liu, Y., Ge, S., Zhao, M., Liu, J., Zhu, A., Meng, X., Yao, Z., and Han, Y.:
1078 Multiproxy reconstruction for Kuroshio responses to northern hemispheric oceanic climate and the
1079 Asian Monsoon since Marine Isotope Stage 5.1 (~88 ka), *Climate of the Past*, 10, 1735-1750, 2014.

1080 Shibahara, A., Ohkushi, K., Kennett, J. P., and Ikehara, K.: Late Quaternary changes in intermediate
1081 water oxygenation and oxygen minimum zone, northern Japan: A benthic foraminiferal perspective,
1082 *Paleoceanography*, 22, PA3213, doi:3210.1029/2005pa001234, 2007.

1083 Shimmiel, G. B. and Price, N. B.: The behaviour of molybdenum and manganese during early
1084 sediment diagenesis — offshore Baja California, Mexico, *Marine Chemistry*, 19, 261-280, 1986.

1085 Sibuet, J. C., Letouzey, J., Barbier, F., Charvet, J., Foucher, J. P., Hilde, T. W. C., Kimura, M., Chiao,
1086 L.-Y., Marsset, B., Muller, C., and Stéphan, J. F.: Back Arc Extension in the Okinawa Trough, *Journal*
1087 *of Geophysical Research: Solid Earth*, 92, 14041-14063, 1987.

1088 Sigman, D. M. and Boyle, E. A.: Glacial/interglacial variations in atmospheric carbon dioxide, *Nature*,
1089 407, 859-869, 2000.

1090 Spratt, R. M. and Lisiecki, L. E.: A Late Pleistocene sea level stack, *Clim. Past*, 12, 1079-1092, 2016.

1091 Sun, Y., Clemens, S. C., Morrill, C., Lin, X., Wang, X., and An, Z.: Influence of Atlantic meridional
1092 overturning circulation on the East Asian winter monsoon, *Nature Geosci*, 5, 46-49, 2012.

1093 Sun, Y. B., Oppo, D. W., Xiang, R., Liu, W. G., and Gao, S.: Last deglaciation in the Okinawa Trough:

1094 Subtropical northwest Pacific link to Northern Hemisphere and tropical climate, *Paleoceanography*, 20,
1095 PA4005, doi:4010.1029/2004pa001061, 2005.

1096 Sundby, B., Martinez, P., and Gobeil, C.: Comparative geochemistry of cadmium, rhenium, uranium,
1097 and molybdenum in continental margin sediments, *Geochimica et Cosmochimica Acta*, 68, 2485-2493,
1098 2004.

1099 Talley, L. D.: Distribution formation of North Pacific Intermediate water, *Journal of Physical*
1100 *Oceanography*, 23, 517-537, 1993.

1101 Talley, L. D.: Hydrographic Atlas of the World Ocean Circulation Experiment (WOCE). In: Volume 2:
1102 Pacific Ocean, Sparrow, M., Chapman, P., and Gould, J. (Eds.), International WOCE Project Office,
1103 Southampton, UK, 2007.

1104 Tribouillard, N., Algeo, T. J., Lyons, T., and Riboulleau, A.: Trace metals as paleoredox and
1105 paleoproductivity proxies: An update, *Chemical Geology*, 232, 12-32, 2006.

1106 Ujiie, H. and Ujiie, Y.: Late Quaternary course changes of the Kuroshio Current in the Ryukyu Arc
1107 region, northwestern Pacific Ocean, *Marine Micropaleontology*, 37, 23-40, 1999.

1108 Ujiie, Y., Asahi, H., Sagawa, T., and Bassinot, F.: Evolution of the North Pacific Subtropical Gyre
1109 during the past 190 kyr through the interaction of the Kuroshio Current with the surface and
1110 intermediate waters, *Paleoceanography*, 31, 1498-1513, 2016.

1111 Ujiie, Y., Ujiie, H., Taira, A., Nakamura, T., and Oguri, K.: Spatial and temporal variability of surface
1112 water in the Kuroshio source region, Pacific Ocean, over the past 21,000 years: evidence from
1113 planktonic foraminifera, *Marine Micropaleontology*, 49, 335-364, 2003.

1114 Vorliceck, T. P. and Helz, G. R.: Catalysis by mineral surfaces: Implications for Mo geochemistry in
1115 anoxic environments, *Geochimica et Cosmochimica Acta*, 66, 3679-3692, 2002.

1116 Wahyudi and Minagawa, M.: Response of benthic foraminifera to organic carbon accumulation rates in
1117 the Okinawa Trough, *Journal of Oceanography*, 53, 411-420, 1997.

1118 Wan, S. and Jian, Z.: Deep water exchanges between the South China Sea and the Pacific since the last
1119 glacial period, *Paleoceanography*, 29, 1162-1178, 2014.

1120 Wang, Y., Cheng, H., Edwards, R. L., He, Y., Kong, X., An, Z., Wu, J., Kelly, M. J., Dykoski, C. A.,
1121 and Li, X.: The Holocene Asian Monsoon: Links to Solar Changes and North Atlantic Climate, *Science*,
1122 308, 854-857, 2005.

1123 Wu, Y., Cheng, Z., and Shi, X.: Stratigraphic and carbonate sediment characteristics of Core CSH1
1124 from the northern Okinawa Trough, *Advances in Marine Science*, 22, 163-169 (in Chinese with English
1125 Abstract), 2004.

1126 Wu, Y., Shi, X., Zou, J., Cheng, Z., Wang, K., Ge, S., and Shi, F.: Benthic foraminiferal $\delta^{13}\text{C}$
1127 minimum events in the southeastern Okhotsk Sea over the last 180ka, *Chinese Science Bulletin*, 59,
1128 3066-3074, 2014.

1129 You, Y. Z.: The pathway and circulation of North Pacific Intermediate Water, *Geophysical Research*
1130 *Letters*, 30, doi:10.1029/2003gl018561, 2003.

1131 You, Y. Z., Suginozawa, N., Fukasawa, M., Yasuda, I., Kaneko, I., Yoritaka, H., and Kawamiya, M.:
1132 Roles of the Okhotsk Sea and Gulf of Alaska in forming the North Pacific Intermediate Water, *Journal*
1133 *of Geophysical Research-Oceans*, 105, 3253-3280, 2000.

1134 You, Y. Z., Suginozawa, N., Fukasawa, M., Yoritaka, H., Mizuno, K., Kashino, Y., and Hartoyo, D.:
1135 Transport of North Pacific Intermediate Water across Japanese WOCE sections, *Journal of Geophysical*
1136 *Research-Oceans*, 108, doi: 10.1029/2002jc001662, 2003.

1137 Yu, H., Liu, Z. X., Berne, S., Jia, G. D., Xiong, Y. Q., Dickens, G. R., Wei, G. J., Shi, X. F., Liu, J. P.,

1138 and Chen, F. J.: Variations in temperature and salinity of the surface water above the middle Okinawa
1139 Trough during the past 37 kyr, *Palaeogeography Palaeoclimatology Palaeoecology*, 281, 154-164,
1140 2009.

1141 Zhang, X., Knorr, G., Lohmann, G., and Barker, S.: Abrupt North Atlantic circulation changes in
1142 response to gradual CO₂ forcing in a glacial climate state, *Nature Geoscience*, 10, 518-524, 2017.

1143 Zheng, X., Kao, S., Chen, Z., Menviel, L., Chen, H., Du, Y., Wan, S., Yan, H., Liu, Z., Zheng, L., Wang,
1144 S., Li, D., and Zhang, X.: Deepwater circulation variation in the South China Sea since the Last Glacial
1145 Maximum, *Geophysical Research Letters*, 43, 8590-8599, 2016.

1146 Zheng, Y., Anderson, R., van Geen, A., and Fleisher, M.: Remobilization of authigenic uranium in
1147 marine sediments by bioturbation, *Geochimica et Cosmochimica Acta*, 66, 1759-1772, 2002.

1148 Zheng, Y., Anderson, R., van Geen, A., and Kuwabara, J.: Authigenic molybdenum formation in marine
1149 sediments: a link to pore water sulfide in the Santa Barbara Basin, *Geochimica et Cosmochimica Acta*,
1150 64, 4165-4178, 2000.

1151 Zhu, A., Shi, X., Zou, J., Wu, Y., Zhang, H., and Bai, Y.: Sediment Provenance and Fluxes in the
1152 Northern Okinawa Trough During the last 88ka, *Marine Geology & Quaternary Geology*, 35, 1-8 (in
1153 Chinese with English Abstract), 2015.

1154 Zou, J., Shi, X., Liu, Y., Liu, J., Selvaraj, K., and Kao, S.-J.: Reconstruction of environmental changes
1155 using a multi-proxy approach in the Ulleung Basin (Sea of Japan) over the last 48 ka, *Journal of*
1156 *Quaternary Science*, 27, 891-900, 2012.

1157

1158 **Captions**

1159 **Table 1.** Locations of different sediment core records and their source references
1160 discussed in the text.

1161

1162 **Table 2.** Age control points adopted between planktic foraminifera species
1163 *Globigerinoides ruber* $\delta^{18}\text{O}$ of Core CSH1 and Chinese stalagmite $\delta^{18}\text{O}$ (Cheng et al.,
1164 2016) for tuning the age model between 10 ka and 60 ka in this study. A linear
1165 interpolation was assumed between age control points.

1166

1167 **Figure 1.** (a) Spatial distribution of dissolved oxygen content at 700 m water depth in
1168 the North Pacific. Black arrows denote simplified Kuroshio and Oyashio circulations
1169 and North Pacific Intermediate Water (NPIW) in the North Pacific. The red thick
1170 dashed line indicates transformation of Okhotsk Sea Intermediate Water (OSIW) by
1171 cabbeling the subtropical NPIW along the subarctic-tropical frontal zone (You, 2003).
1172 The light brown solid line with arrow indicates the spreading path of subtropical
1173 NPIW from northeast North Pacific southward toward the low-latitude northwest
1174 North Pacific (You, 2003). Yellow solid lines with arrow represent two passages
1175 through which NPIW enter into the Okinawa Trough. This figure was created with
1176 Ocean Data View (odv.awi.de). (b) Location of sediment core CSH1 investigated in
1177 this study (red diamond). Also shown are locations of sediment cores PN-3, E017, 255
1178 and MD012404 investigated previously from the Okinawa Trough, GH08-2004 from
1179 the East of Ryukyu Island, GH02-1030 off the east of Japan, PC-23A from the Bering
1180 Sea and ODP167-1017 from the northeastern Pacific. Letters A to E represent the
1181 sediment cores from and near the OT. The detailed information for these cores is
1182 shown in Table 1.

1183

1184 **Figure 2.** Spatial distribution of sea surface salinity in the East China Sea. (a) summer
1185 (July to September); (b) winter (January to March). Lower sea surface salinity in
1186 summer relative to that of winter indicates strong effects of summer East Asian
1187 Monsoon.

1188

1189 **Figure 3.** (a) Lithology and oxygen isotope ($\delta^{18}\text{O}$) profile of planktic foraminifera
1190 species *Globigerinoides ruber* (*G.ruber*) in core CSH1. (b) Plot of ages versus depth
1191 for core CSH1. Three known ash layers are indicated by solid red rectangles. (c) Time
1192 series of linear sedimentation rate (LSR) from core CSH1. (d) Comparison of age
1193 model of core CSH1 with Chinese Stalagmite composite $\delta^{18}\text{O}$ curve of (Cheng et al.,
1194 2016). Tie points for CSH1 core chronology (Table 2) in Figures 3c and 3d are
1195 designated by colored crosses.

1196

1197 **Figure 4.** Age versus (a) CaCO_3 concentration, (b) Total nitrogen (TN) concentration,
1198 (c) Total organic carbon (TOC) concentration, (d) C/N molar ratio, (e) linear
1199 sedimentation rate (LSR), (f) Al concentration, (g) Mn concentration, (h) Mo/Mn ratio,
1200 (i) Mo concentration, (j) excess Mo concentration, (k) U concentration and (l) excess
1201 U concentration and (m) $(\text{Mo}/\text{U})_{\text{excess}}$ ratio in core CSH1. Light gray and dark gray
1202 vertical bars indicate different sediment intervals in core CSH1. 8.2 ka, PB, YD, B/A,
1203 HS1, LGM and HS2 refer to 8,200 year cold event, Preboreal, Younger Dryas, Bölling
1204 - Alleröd, Heinrich Stadial 1, Last Glacial Maximum and Heinrich Stadial 2,
1205 respectively, which were identified in core CSH1. Blue solid diamonds in Figure 4m
1206 indicate the age control points.

1207

1208 **Figure 5.** Scatter plots of $\text{Mo}_{\text{excess}}$ vs Mn concentrations and U_{excess} concentration vs
1209 Mo/Mn ratio at different time intervals in core CSH1. A various correlation is present
1210 in core CSH1 at different time intervals, which shows their complicated geochemical
1211 behaviors (Figs.5a and 5b). Strong positive correlation between Mo/Mn ratio and
1212 U_{excess} concentration (Fig.5c) suggest that Mo/Mn ratio is a reliable proxy to track
1213 sedimentary redox conditions in the geological past.

1214

1215 **Figure 6.** Proxy-related reconstructions of mid-depth sedimentary oxygenation at site
1216 CSH1 (this study) compared with oxygenation records from other locations of the
1217 North Pacific and published climatic and environmental records from the Okinawa

1218 Trough. From top to bottom: (a) CaCO₃ concentration, (b) U_{excess} concentration, (c)
1219 Mo/Mn ratio, and (d) sea surface temperature (SST) (Shi et al., 2014), (e) abundance
1220 of *P.obliquiloculata* in core CSH1 (Shi et al., 2014), (f) bulk sedimentary organic
1221 matter δ¹⁵N in core MD01-2404 (Kao et al., 2008), (g) δ¹³C of epibenthic
1222 foraminiferal *C.wuellerstorfi* in core PN-3 (Wahyudi and Minagawa, 1997), (h)
1223 relative abundance of *B. aculeata* (hypoxia-like species) and (i) *C.hyalinea*
1224 (oxygen-like species) (Li et al., 2005), (j) dysoxic taxa (%) in core ODP 167-1017 in
1225 the northeastern Pacific (Cannariato and Kennett, 1999) and (k) δ¹³C of benthic
1226 foraminiferal *Uvigerina akitaensis* in core PC23A in the Bering Sea (Rella et al.,
1227 2012). Light gray and dark gray vertical bars are the same as those in Figure 4.

1228

1229 **Figure 7.** Proxy records favoring the existence of out-of-phase connections between
1230 the subtropical North Pacific and North Atlantic during the last deglaciation and
1231 enhanced carbon storage at mid-depth waters. (a) U_{excess} concentration in core CSH1;
1232 (b) Mo/Mn ratio in core CSH1; (c) benthic δ¹³C record in core PC-23A in the Bering
1233 Sea (Rella et al., 2012); (d) Indicator of strength of Atlantic Meridional Ocean
1234 Circulation (²³¹Pa/²³⁰Th) (Böhm et al., 2015; McManus et al., 2004); (e) Atmospheric
1235 CO₂ concentration (Marcott et al., 2014). Light gray and dark gray vertical bars are
1236 the same as those in Figure 4.

1237

Table 1

Label in Figure 1b	Station	Latitude (°N)	Longitude (°E)	Water depth (m)	Area	Reference
	CSH1	31.23	128.72	703	Okinawa Trough	this study
A	PN-3	28.10	127.34	1058	Okinawa Trough	Wahyudi and Minagawa, (1997)
B	MD012404	26.65	125.81	1397	Okinawa Trough	Kao et al., (2008)
C	E017	26.57	126.02	1826	Okinawa Trough	Li et al., (2005)
D	255	25.20	123.12	1575	Okinawa Trough	Jian et al., (1996)
E	GH08-2004	26.21	127.09	1166	East of Ryukyu Island	Kubota et al. (2015)
	GH02-1030	42.23	144.21	1212	Off Japan	Sagawa and Ikehara, (2008)
	PC-23A	60.16	179.46	1002	Bering Sea	Rella et al.,(2012)
	ODP167-1017	34.54	239.11	955	NE Pacific	Cannariato and Kennett, (1999)

1 Table 2

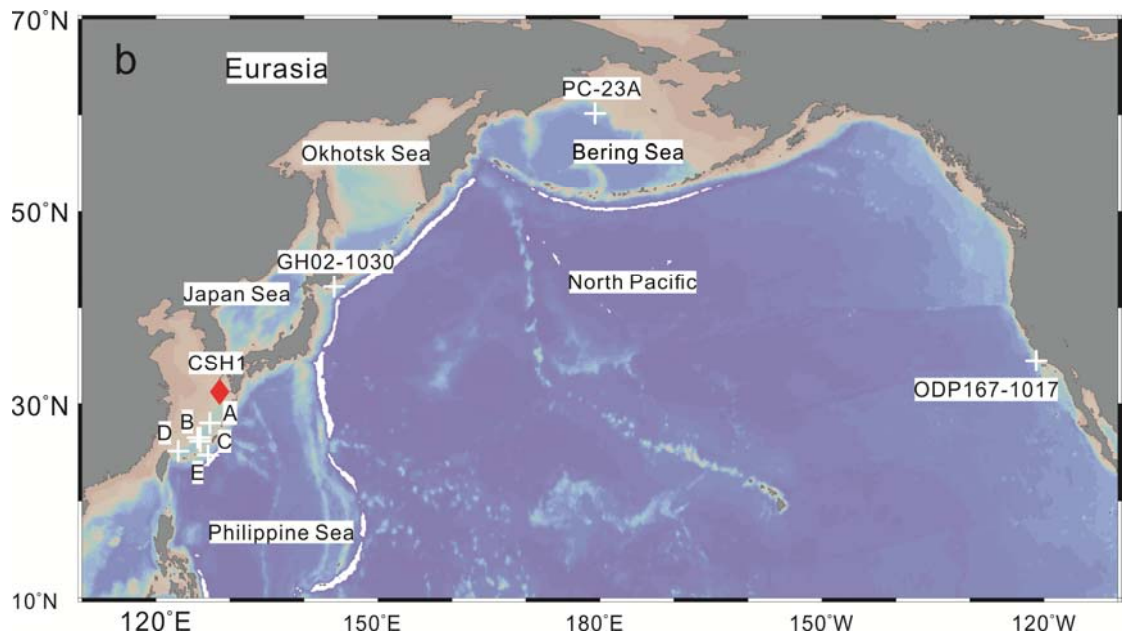
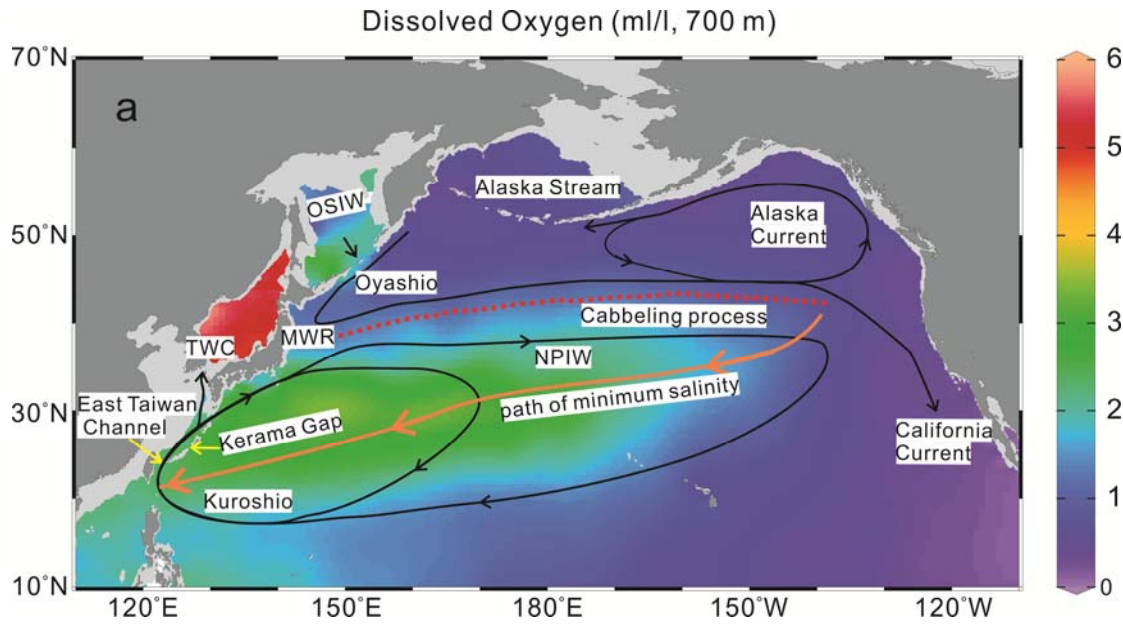
2

Depth(cm)	AMS ¹⁴ C (yr)	Error (yr)	Calibrated Age (yr)	Tie Point Type	LSR (cm/ka)	Source
10	3420	±35	3296	¹⁴ C		Shi et al., (2014)
106	7060	± 40	7545	¹⁴ C	22.59	Shi et al., (2014)
218			12352	Stalagmite, YD	23.30	This study
322			16029	Stalagmite, H1	28.28	This study
362			19838	Stalagmite	10.50	This study
506			24163	Stalagmite, H2	33.29	This study
698			28963	Stalagmite, DO4	40.00	This study
834			32442	Stalagmite, DO5	39.09	This study
938			37526	Stalagmite, DO8	20.46	This study
978			39468	Stalagmite, H4	20.60	This study
1058			46151	Stalagmite, DO12	11.97	This study
1122			49432	Stalagmite, DO13	19.51	This study
1242			52831	Stalagmite, DO14	35.30	This study
1282			57241	Stalagmite, DO16	9.07	This study
1346			61007	Stalagmite, H6	16.99	This study
1530		±2590	73910	MIS4/5	14.26	Shi et al., (2014)
1610		±3580	79250	MIS 5.1	14.98	Shi et al., (2014)

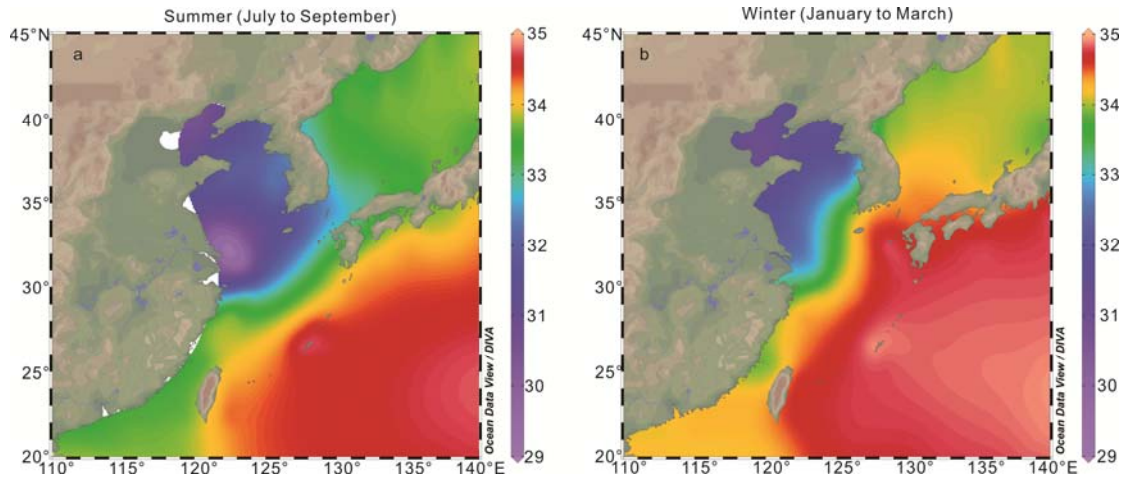
3

4

5 Fig.1



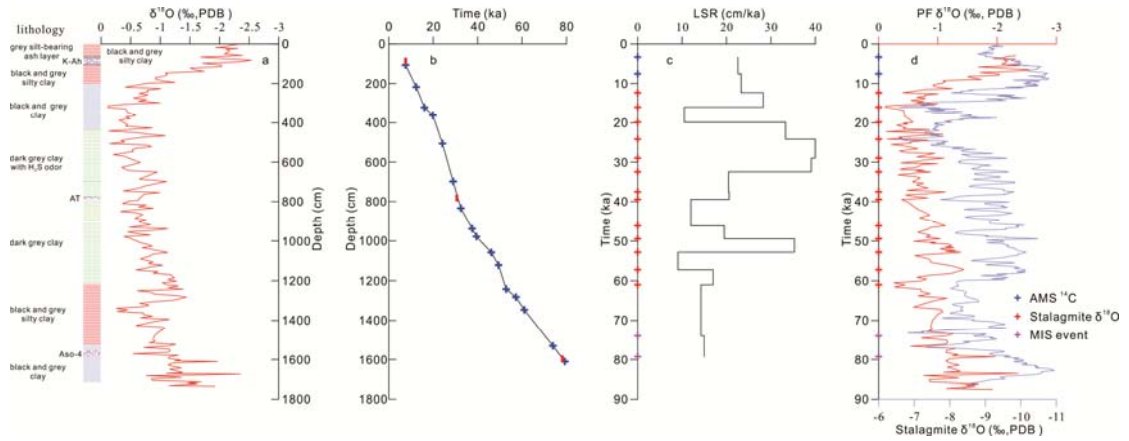
11 Fig.2



12

13

14 Fig.3

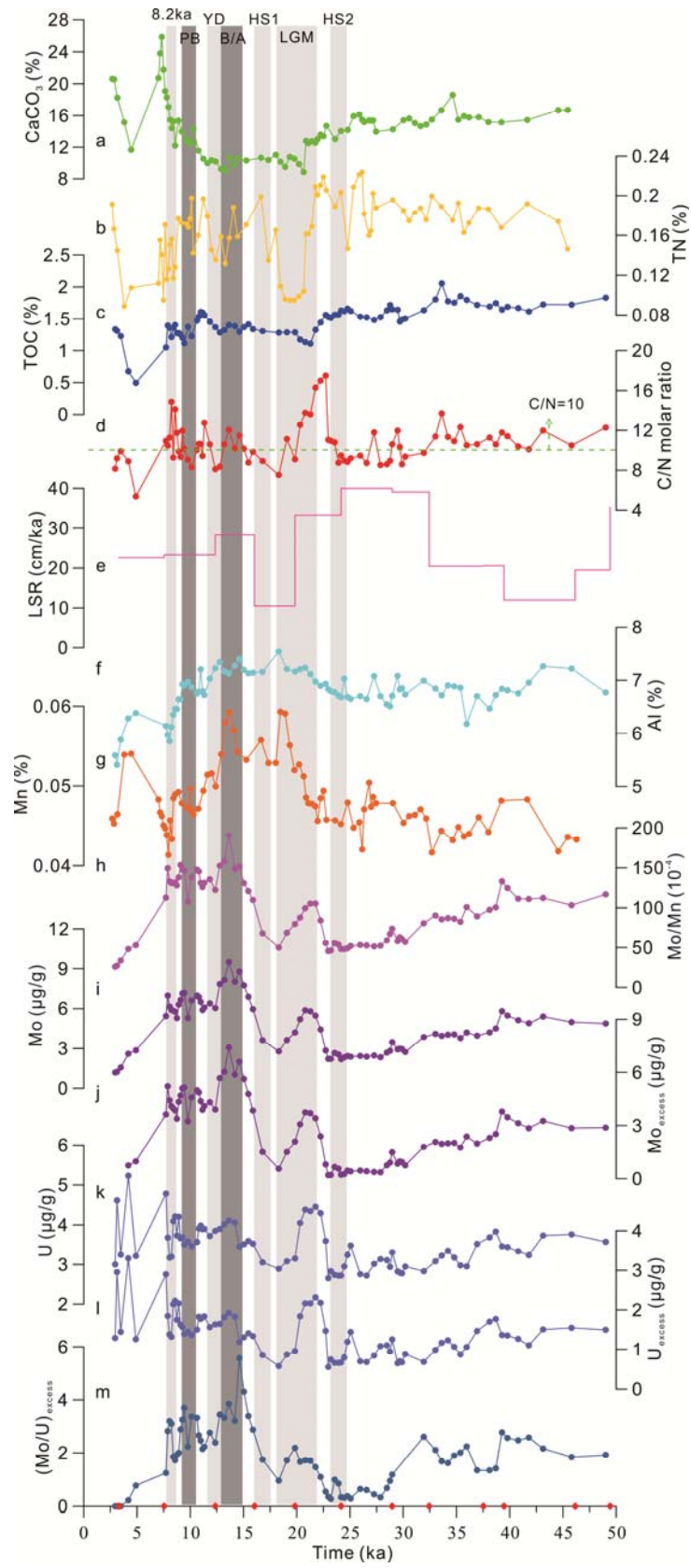


15

16

17

18 Fig.4

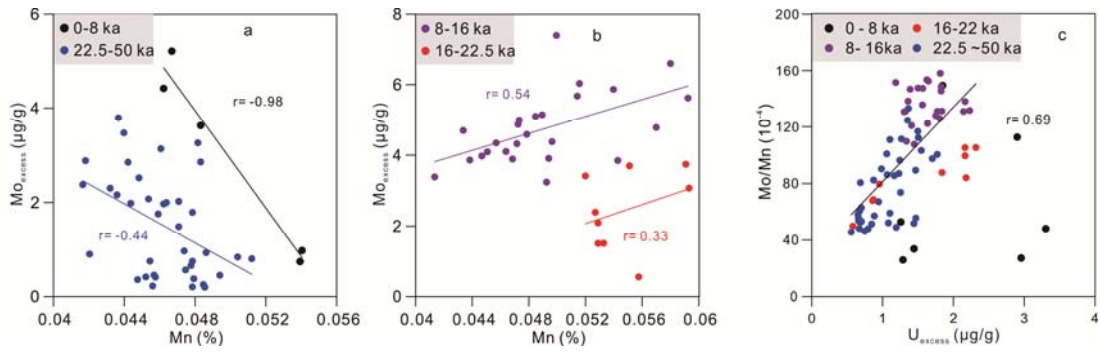


19

20

21 Fig.5

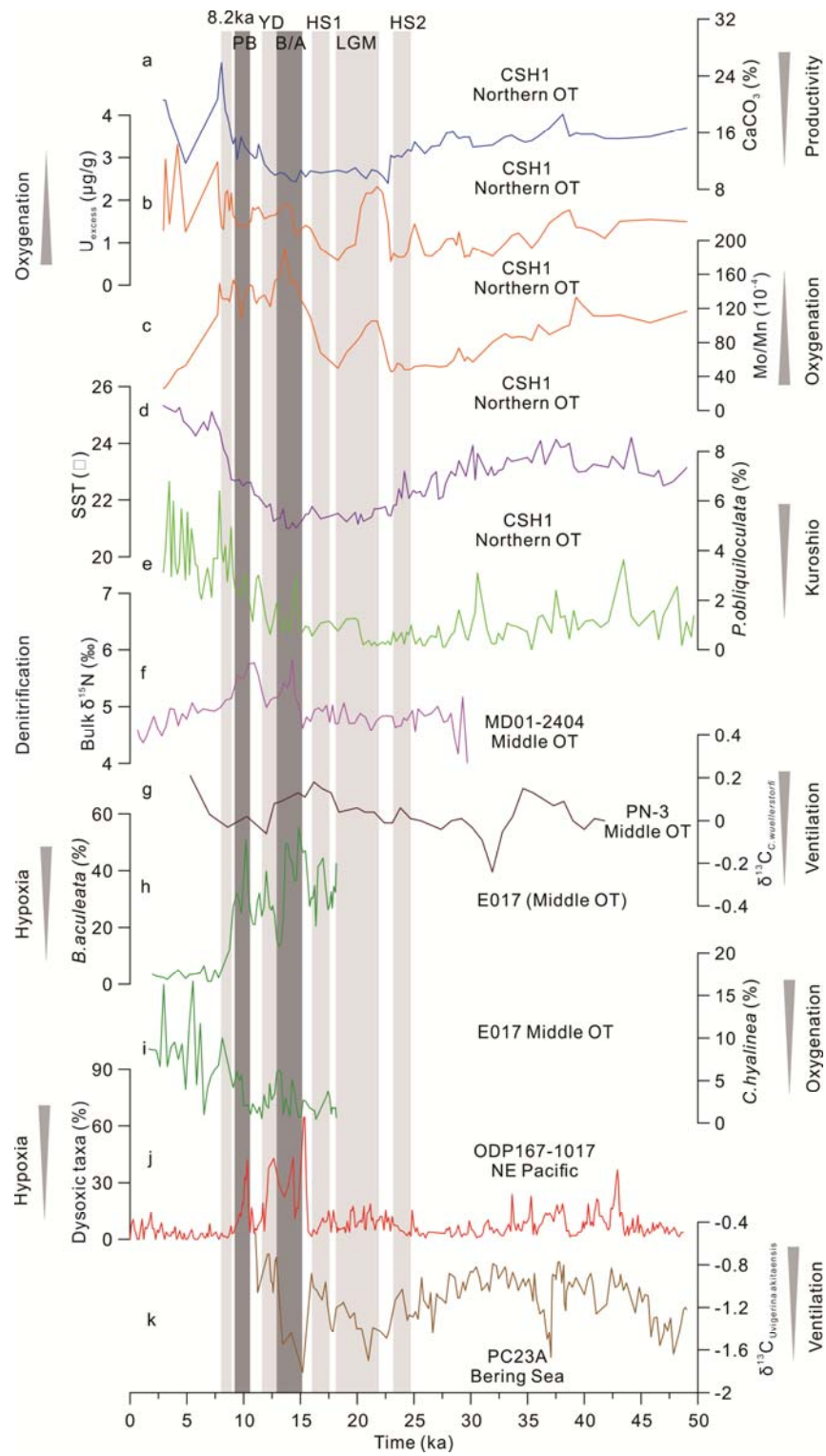
22



23

24

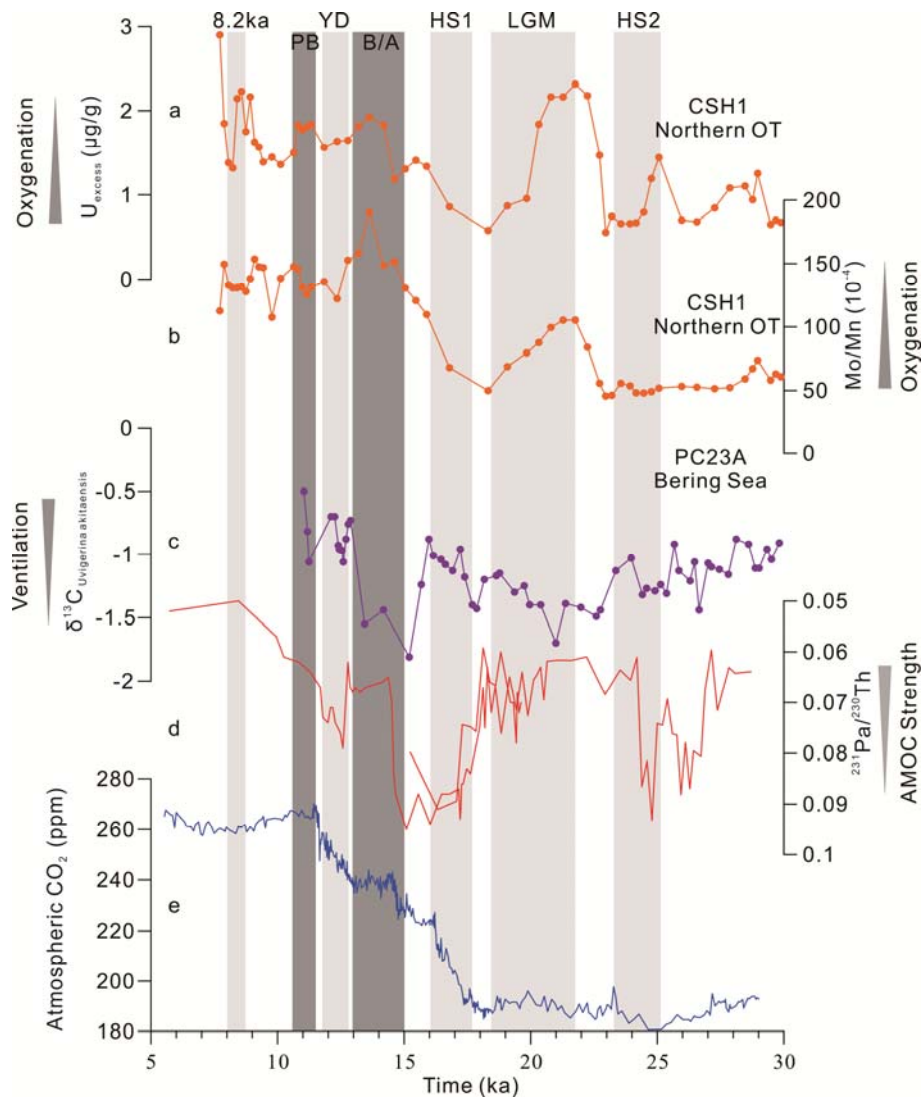
25 Fig.6



26

27

28 Fig.7



29

30